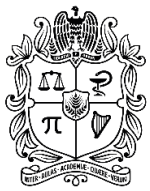

UNIVERSIDAD
NACIONAL
DE COLOMBIA

Direct Detection with phase recovery in optical communications

Diego Alejandro Figueroa Del Castillo

Universidad Nacional de Colombia
Facultad de Ingenieria , Departamento de Eléctrica y Electrónica
Bogotá, Colombia
December, 2023

This page intentionally left blank.

Acknowledgments

I want to thank my family for the support, my friends for accompanying me during my studies and motivating me to do the best I could, the National University of Colombia and the CMUN for cultivating my knowledge, and the Karlsruhe Institute of Technology and the CEL institute for welcoming me and guiding me during the work of this report.

This page intentionally left blank.

Abstract

In this report, we introduce the phase recovery problem in optical communications with Direct Detection (DD), review some papers that study the information capacity of channels under DD, and show that the capacity loss is at most 1 bit compared with the coherent detection. Then, we review two proposed systems that try to recover the phase when using DD. Finally, we propose a detector for one of these systems based on machine learning with the hope of reducing the complexity of the decoder. Unfortunately, the performance of the proposed decoder, in terms of the SER, is not as good as expected because the decoder presents a high error floor. However, it opens the door for exploring decoders based on machine learning, so we propose some possible future work for testing different architectures.

This page intentionally left blank.

Contents

Abstract **iii**

List of Figures **vi**

List of Tables **ix**

List of symbols, abbreviations and notation **xi**

1 Introduction **1**
1.1 Direct Detection . . . 1
1.2 Capacity under direct detection . . . 2
1.3 Basic principle of phase recovery . . . 3

2 Tukey signaling **5**
2.1 System model . . . 5
2.1.1 Dispersion precompensation . . . 5
2.1.2 Transmission medium . . . 6
2.1.3 Photodiode . . . 6
2.1.4 Signaling . . . 6
2.1.5 Integrate and dump . . . 8
2.1.6 Class representative . . . 9
2.1.6.1 Analysis on ambiguities . . . 9
2.1.7 Detector . . . 12
2.2 Numerical simulation . . . 13
2.2.1 System parameters . . . 13
2.2.2 Class representative creation . . . 13
2.2.3 Mutual information estimation . . . 14
2.2.4 BER estimation . . . 16
2.3 Discussion . . . 16

3 Generalized Direct Detection with phase recovery **19**
3.1 System model . . . 19
3.1.1 Continuous time Model . . . 19

3.1.1.1 Differential encoder . . . 19
3.1.1.2 Transmitter . . . 20
3.1.1.3 Fiber Optic Link . . . 20
3.1.1.4 Receiver . . . 20
3.1.2 Discrete time Model . . . 21
3.1.2.1 Discrete signal notation . . . 21
3.1.2.2 Vector matrix notation . . . 21
3.1.2.3 Even and odd samples . . . 22
3.1.3 Symbol-wise MAP detection . . . 23
3.2 Numerical simulation . . . 24
3.3 Discussion . . . 26

4 MagPhase-DetNet **27**
4.1 Separation in even and odd subchannel . . . 28
4.2 Real and imaginary reparametrization . . . 28
4.3 MagPhase-DetNet architecture . . . 29
4.3.1 Magnitude phase reparametrization . . . 30
4.3.2 Magnitude DetNet block . . . 31
4.3.3 Phase DetNet block . . . 32
4.4 Numerical simulation . . . 34
4.4.1 Training process . . . 34
4.4.1.1 Hyper parameters . . . 34
4.4.1.2 Training set . . . 34
4.4.2 Evaluation process . . . 34
4.4.2.1 Simple evaluation . . . 34
4.4.2.2 Sequential evaluation . . . 35
4.5 Conclusions . . . 36

Bibliography **39**

List of Figures

1.1 Comparative of the waveforms under coherent detection and direct detection. Based on [6], [7]. 4

2.1 System model for Tukey signaling. Based on [1]. 5
2.2 Tukey window for different β, $\beta_1 < \beta_2$. Based on [1]. 7
2.3 ISI-free and ISI-pressent intervals for $n = 3$. Based in [1]. 8
2.4 Construction of 4 different but square law equivalent symbol blocks. 10
2.5 Construction of 4 new different but square law equivalent symbol blocks by reflection. 11
2.6 Construction of 32 new different but square law equivalent symbol blocks by rotation. 12
2.7 All the symbol blocks in an equivalence class shown at the same time. 12
2.8 Different possible constellations $\mathcal{K}$. 14
2.9 Mutual information of the system with 2-ring 4-ary phase constellation and symbol block length $n = 3$. 16
2.10 Bit error rate of the system with 2-ring 4-ary phase constellation and symbol block length $n = 4$. 17

3.1 System model proposed in [7]. 19
3.2 Differential phase mapper example for M-ASK. Based on [9]. 20
3.3 Signals for oversampling factor $N_{\text{os}} = 2$. Based on [7]. 23
3.4 Factor graph to implement the BCJR. Based on [7]. 23
3.5 Simulated and auxiliary channel. Based on [7]. 25
3.6 DD-SQAM constellation. 25
3.7 Symbol error rate vs SNR for different constellations and channel lengths. . . 26

4.1 MagPhase-DetNet architecture. 30
4.2 Evaluation method used for the simple evaluation of the MagPhase-DetNet. Example for $\widetilde{M} = 3$. 35
4.3 Simple evaluation of the MagPhase-DetNet trained for different SNR and channel memory. The dotted lines are the reference optimal performance. 35
4.4 Evaluation method used for the sequential evaluation of the MagPhase-DetNet. Example for $\widetilde{M} = 3$. 36

4.5 Sequential evaluation of the MagPhase-DetNet trained for different SNR and channel memory. The dotted lines are the reference optimal performance. . . 36

List of Tables

2.1 Bandwidth containing 95% of the waveform energy, and the overhead compared to the minimum bandwidth for Nyquist signaling. Taken from [1]. . . . 8
2.2 Parameter of the photodiode used in the simulations. Taken from [1]. . . . 13
2.3 Number of equivalence classes for 4-PSK constellation. 14
2.4 Number of equivalence classes for 2-ring 4-ary Phase constellation. 15
2.5 Number of equivalence classes for 5-ring 5-ary Phase constellation. 15
2.6 Number of equivalence classes for different constellations. 15

3.1 Simulation parameters. Taken from [7]. 25

This page intentionally left blank.

List of symbols, abbreviations and notation

Probability theory

PDF	Probability density function	page 13
i.i.d.	independent and identically distributed	page 20
$\mathbb{E}[X]$	Expected value of X	page 24
$X \sim \mathcal{N}(\mu, \sigma^2)$	X has a Gaussian distribution with mean μ and variance σ^2	page 8
$\mathcal{N}(x; \mu, \sigma^2)$	Univariate real Gaussian distributions, with mean μ and variance σ^2.	page 22
$\mathcal{N}(\boldsymbol{x}; \boldsymbol{\mu}, \boldsymbol{C})$	Multivariate real Gaussian distributions, with mean vector μ and covariance matrix $\boldsymbol{C}$.	page 22

Mathematics

$\mathrm{Re}\{z\}$	Real part of z	page 3
$\mathrm{Im}\{z\}$	imaginary part of z	page 3
$\mathbf{0}_n$	Ceros vector of length n	page 22
$\boldsymbol{I}_n$	Identity matrix of size $n \times n$	page 22
$\mathrm{diag}(\boldsymbol{x})$	Diagonal matrix with the elements of $\boldsymbol{x}$ along the diagonal	page 31
$\odot$	Element wise multiplication	page 31
$\mathrm{sinc}(t)$	$\frac{\sin(\pi t)}{\pi t}$	page 4
$\mathcal{F}\{\cdot\}$	Fourier transform	page 6
$\mathcal{F}^{-1}\{\cdot\}$	Inverse fourier transform	page 6
$\lvert\cdot\rvert^{\circ 2}$	Element wise $\lvert\cdot\rvert^2$ operator	page 22

Constants

j	Imaginary unit	page 3

k_b	Boltzmann constant	page 2
q	Electron charge	page 2

Variables

f	Frequency	page 6
β_2	Group-velocity dispersion parameter	page 6

Others

DD	Direct Detection	page 1
SQL	Square law	page 1
SLD	Square law detection	page 19
IM-DD	Intensity modulation - Direct detection	page 30
ISI	Inter symbol Interference	page 3
ROP	Received optical power	page 15
SNR	Signal to noise ratio	page 15
MAP	Maximum a posteriori probability	page 23
APP	a posteriori probability	page 23
BER	Bit error rate	page 16
SER	Symbol error rate	page 24
MI	Mutual information	page 14
APD	Avalanche photodiode	page 6
MIMO	Multiple input multiple output	page 27
AWGN	Additive white Gaussian noise	page 27

Chapter 1

Introduction

Square-law (SQL) detection, also known as Direct detection (DD), is a detection scheme that measures the square magnitude of a complex waveform; clearly, this scheme is a nonlinear waveform detection because of the square operation. Direct detection is widely used in different scientific fields, such as crystallography, radio astronomy, and biomedical spectroscopy, among others [1]. In particular, this scheme is often used in optical communications, especially in short-haul systems with length up to 50 km [2] due to its simplicity, or even in shorter links up to 10 km, for example in rack to rack communications in big data centers [1].

In recent years, the interest in studying systems with DD is getting bigger again because of the simplicity of the receivers, which are a promising low-cost alternative compared to the coherent detection systems [3]. In this context, two questions or problems arise. First, how good is a system with DD compared to a system with coherent detection in terms of the information capacity of the channel. And second, how to design a system that exploits the information capacity of the DD channel in the best possible way.

In this work, we briefly cover two answers to the first question, and then we review two systems proposed for a channel with DD. Then, we try to propose a new decoder for the second system, with reduced complexity at the expense of a slightly worse performance.

1.1 Direct Detection

In optical communication, DD is performed with a single photodiode that converts the optical signal into an electric signal through the photoelectric effect according to the next equation [4]:

$$I_p = R_d \cdot P_{in} \tag{1.1}$$

where I_p is the photocurrent, P_{in} is the incident optical power (which is proportional to the square of the magnitude of the electric field, that is where the square-law term comes from),

and R_d is the so-called responsivity of the photodetector, with units of A/W.

The noise in the photodiode is generated primarily by two mechanisms: in the first place, the shot noise, and in the second place, thermal noise.

The shot noise models the fact that the photocurrent consists of a stream of electrons generated at random times. Mathematically, the current corresponding to the shot noise $i_s(t)$ is a stationary random process with Poisson distribution but is usually approximated by a Gaussian distribution with variance given by [4]:

$$\sigma_s^2 = 2qI_pB \tag{1.2}$$

where q is the electron charge, I_p the photocurrent, and B the bandwidth of the system. σ_s can be interpreted as the RMS value of the shot noise current $i_s(t)$.

The thermal noise is generated by the movement of electrons due to the ambient temperature; this kind of noise is Gaussian distributed, and its variance is given by [4]:

$$\sigma_{th}^2 = \frac{4k_BT}{R_L}F_nB \tag{1.3}$$

where k_B is the Boltzmann constant, T is the temperature given in kelvin, R_L is the load resistance, B the bandwidth, and F_n is the amplifier noise figure.

With this in mind, the output current of the direct detection process is given by:

$$I(t) = I_p + i_s(t) + i_{th}(t) \tag{1.4}$$

with $i_s(t) \sim \mathcal{N}(0, \sigma_s^2)$ and $i_{th}(t) \sim \mathcal{N}(0, \sigma_{th}^2)$.

1.2 Capacity under direct detection

A communications channel that uses DD can retrieve only the information about the magnitude of the signal; in contrast, a system with coherent detection can retrieve the magnitude and phase of the signal. This means that the DD scheme ignores one of the two degrees of freedom, and hence, it is reasonable to think that the capacity of this system should be approximately half that of the system with coherent detection [1], [3], [5].

However, in [3], it is shown that the spectra efficiency of a band-limited system under DD is at most 1 bit/s/Hz less than the same system under coherent detection. Also, in [5], it is proven that for time-limited signals, the capacity is also at most one bit less than the coherent case. This means that contrary to intuition, the loss in the capacity of a system under DD is not half of the coherent system, but just 1 bit/s/Hz.

The results of these papers show that the systems with DD have a considerable potential because the detector is cheaper and easier to implement (basically just one photodiode), and the loss in the capacity may be smaller than thought. However, the problem of finding a system simple enough that uses the potential of the DD is still open.

1.3 Basic principle of phase recovery

The key to retrieve the phase information of the transmitted symbols when using DD is to use the ISI. As a toy example, one can think of the problem where given two complex numbers z_1 and z_2; from $|z_1|^2$, $|z_2|^2$ and $|z_1 + z_2|^2$ (an ISI term), it is possible to determine the phase difference between z_1 and z_2 up to a sign ambiguity [1].

To show this, notice the following:

$$\begin{aligned} |z_1 + z_2|^2 &= (z_1 + z_2)(z_1 + z_2)^* \\ &= z_1 z_1^* + z_1 z_2^* + z_2 z_2^* + z_1^* z_2 \\ &= |z_1|^2 + |z_2|^2 + z_1 z_2^* + \left(z_1 z_2^*\right)^* \\ &= |z_1|^2 + |z_2|^2 + 2\mathrm{Re}\{z_1 z_2^*\} \end{aligned}$$

under the convention that $z_1 = a \cdot e^{j\alpha}$ and $z_2 = b \cdot e^{j\beta}$

$$|z_1 + z_2|^2 = |z_1|^2 + |z_2|^2 + 2|z_1||z_2| \cos(\alpha - \beta) \tag{1.5}$$

Clearly if $|z_1|^2$, $|z_2|^2$ and $|z_1+z_2|^2$ are known, one can solve the equation 1.5 for $\cos(\alpha-\beta)$ and get the information about the phase difference between z_1 and z_2. However, since cosine is an even function $\cos(\alpha - \beta) = \cos(-\alpha + \beta)$, hence there is still an ambiguity on the sign of the phase difference.

To visualize this principle in a real system (jet not even near optimal due to the big bandwidth of the pulse), see figure 1.1. There is shown with a solid line the waveform of a simple transmission under coherent detection (see figure 1.1a) and under direct detection (see figure 1.1b), and also the waveform of the individual transmitted symbols in dashed lines.

For the coherent detection case, the samples at each symbol time are sufficient to determine the transmitted symbols. In contrast, for the direct detection case, the samples at each symbol time (circles) only carry information about the magnitude of the symbols (always one in this example), and the samples at intermediate symbol time (squares) carry information about the phase difference [6].

Figure 1.1c shows the DD system for a longer sequence. There it is possible to notice that the even samples always carry information about the magnitude, whereas the odd samples carry information about the differential phase of the symbols. This toy example shows the principle behind phase recovery in DD systems.

It is important to highlight two things: first, an oversampling factor of two is needed, and second, only information on the differential phase (up to a sign ambiguity) is retrieved. Hence, it is beneficial to use differential coding in the transmission.

Another way to explain the previous conclusions is to take a look at the simple system given by:

$$g(t) = \sum_{k=0}^{m} g_k \mathrm{sinc}(t - k)$$

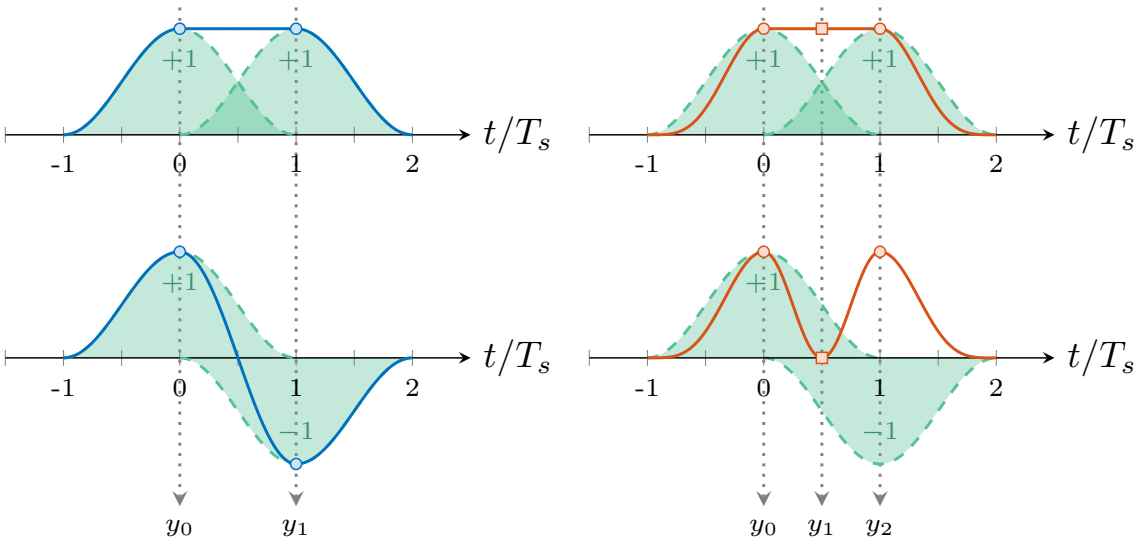

(a) Coherent detection

(b) Direct detection

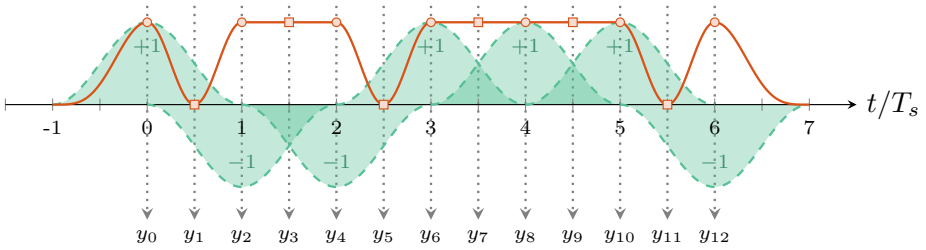

(c) Direct detection of the sequence $\{+1, -1, -1, +1, +1, +1, -1\}$

Figure 1.1: Comparative of the waveforms under coherent detection and direct detection. Based on [6], [7].

where g_k is a complex number representing the k-th transmitted symbol, and $g(t)$ is the transmitted signal. Note that after the DD, the bandwidth of the signal is twice as big as the bandwidth of $g(t)$ since the received signal is given by the product $|g(t)|^2 = g(t)g^*(t)$. Hence, to recover the data, one should use an oversampling factor of two, so the sampled signal becomes [1]:

$$\left|g\left(\frac{n}{2}\right)\right|^2 = \begin{cases} \left|g_{\frac{n}{2}}\right|^2 & \text{if } n \text{ is even} \\ \left|\sum_{k=0}^{m} g_k \text{sinc}\left(\frac{n}{2} - k\right)\right|^2 & \text{if } n \text{ is odd} \end{cases} \qquad \text{for } n = 0, \cdots, 2m$$

Once again, it is clear that the even samples carry the information about the magnitude of the symbols. In contrast, the odd samples have somehow the information about the phase of the symbols, but now notice that all the g_k contribute to the odd samples. As we will see in later chapters, retrieving the phase quickly becomes an intractable problem as m grows [1].

Chapter 2

Tukey signaling

One of the solutions given to the problem of phase recovery under DD is the so-called Tukey signaling proposed in [1]. The main idea of this paper is to introduce controlled ISI in the transmission and use the interference between symbols to recover the phase of the symbols in a block of length n symbols. The system is proposed for short-haul systems, specifically for links with lengths less than 10 km.

The system model proposed in the paper is shown in figure 2.1. In the following sections, each block will be explained and discussed when needed. Nevertheless, the blocks will be described in a different order to facilitate understanding. First, the dispersion precompensation, the transmission medium, and the photodiode will be explained, then the signaling block, integrate and dump, class representative, and finally, the decoder.

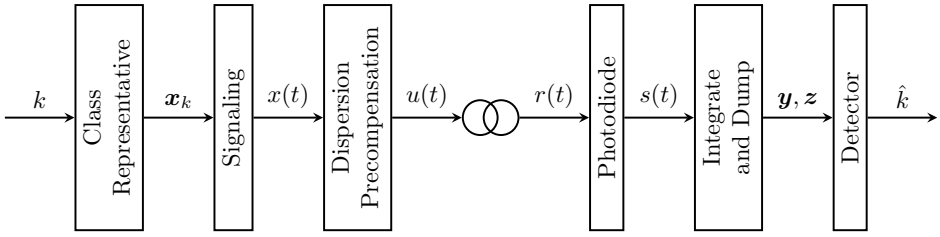

Figure 2.1: System model for Tukey signaling. Based on [1].

2.1 System model

2.1.1 Dispersion precompensation

In this block, the chromatic dispersion of the optical fiber is precompensated by an all-pass filter with a transfer function given by [1]:

$$H(f) = e^{j2\beta_2 L\pi^2 f^2} \tag{2.1}$$

where β_2 is the group-velocity dispersion parameter and L is the fiber length [1].

Clearly, from this description of the block, the following relations between $x(t)$ and $u(t)$ are given:

$$u(t) = \mathcal{F}^{-1}\{X(f)H(f)\} \tag{2.2}$$

where $X(f)$ is the Fourier transform of $x(t)$

2.1.2 Transmission medium

Since the optical fiber length is less than 10 km, it is possible to ignore all the transmission impairments, except for power loss and chromatic dispersion [1]. With this in mind and taking into account the dispersion pre-compensation, we have the following relation:

$$r(t) = \rho x(t) \tag{2.3}$$

where $0 < \rho \leq 1$ is the attenuation constant, depending on the fiber's length. The particular case $\rho = 1$, i.e. without attenuation, is called back-to-back transmission.

2.1.3 Photodiode

An avalanche photodiode (APD) is used for this system, and this diode is considered the only noise source. In this case, both shoot and thermal noise are considered. The behavior of the diode is given by [1]:

$$s(t) = |r(t)|^2 + |r(t)|n_{sh}(t) + n_{th}(t) \tag{2.4}$$

where $n_{sh}(t)$ and $n_{th}(t)$ are Gaussian distributed, and the variance of each noise is given by [1]:

$$\sigma_{th}^2 = \frac{4k_B T B}{R_L} \tag{2.5}$$

$$\sigma_{sh}^2 = 2qM_{\text{APD}}^2 F R_{\text{APD}} B \tag{2.6}$$

Notice that the difference between the σ_{sh}^2 presented here and the equation 1.2 is due to the gain of the APD.

2.1.4 Signaling

This block receives n complex numbers $x_0, \ldots, x_{n-1}$, which are the transmitted symbols, and produces a continuous time complex signal given by:

$$x(t) = \sum_{i=0}^{n-1} x_i w(t - iT) \tag{2.7}$$

where T is the inverse of the baud rate and $w(t)$ is a waveform.

Usually, in communications, $w(t)$ is a root raised-cosine waveform, however the ISI of this pulse at times different from the symbol time is too complicated because a lot of symbols interfere, if not all of them, and that makes the problem of recovering the phase to complicated. That is why the paper proposes a time-limited waveform with a simpler "ISI pattern".

The proposed waveform is the Tukey window, which is equivalent to the Fourier transform of a raised cosine but in the time domain. This waveform is given by:

$$w_\beta(t) = \begin{cases} \frac{2}{\sqrt{4-\beta}} & \text{if } |t| \leq \frac{1-\beta}{2} \\ \frac{1}{\sqrt{4-\beta}} \left(1 - \sin\left(\frac{\pi(2|t|-1)}{2\beta}\right)\right) & \text{if } \left||t| - \frac{1}{2}\right| \leq \frac{\beta}{2} \\ 0 & \text{otherwise} \end{cases} \tag{2.8}$$

$$W_\beta(f) = \begin{cases} \frac{\pi}{2\sqrt{4-\beta}} \cdot \operatorname{sinc}\left(\frac{1}{2\beta}\right) & \text{if } f = \pm\frac{1}{2\beta} \\ \frac{2}{\sqrt{4-\beta}} \cdot \operatorname{sinc}(f) \cdot \frac{\cos(\pi\beta f)}{1-(2\beta f)^2} & \text{otherwise} \end{cases} \tag{2.9}$$

Notice that the factor $2/\sqrt{4-\beta}$ is to normalize the energy of the waveform.

The waveform can be seen in figure 2.2 both in the time domain and frequency domain for two different β.

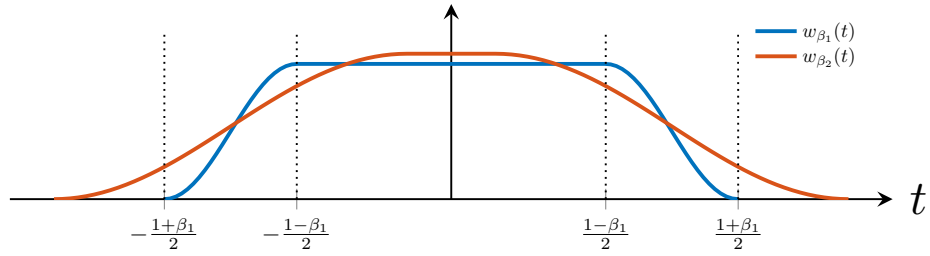

(a) Time domain

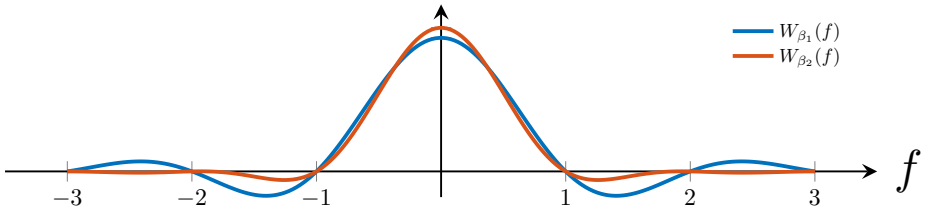

(b) Frequency domain

Figure 2.2: Tukey window for different β, $\beta_1 < \beta_2$. Based on [1].

When we select $w(t) = w_\beta(t/T)$ in equation 2.7, the resulting signal have an important property: at any given time, either only one or only two symbols contribute to the value of the signal; here we see the meaning of *controlled* ISI. According to this property, we define two types of intervals: an ISI-free interval $\mathcal{Y}_i$, where $x(t)$ depends only on x_i, and an ISI-present interval $\mathcal{Z}_i$, where $x(t)$ depends only on x_i and x_{i+1}. Those intervals are shown in the figure 2.3 and are given by:

$$\mathcal{Y}_i : \left[\left(i - \frac{1-\beta}{2}\right)T, \left(i + \frac{1-\beta}{2}\right)T\right] \qquad i \in \{0, \ldots, n-1\} \tag{2.10}$$

$$\mathcal{Z}_i : \left[\left(i + \frac{1-\beta}{2}\right)T, \left(i + \frac{1+\beta}{2}\right)T\right] \qquad i \in \{0, \ldots, n-2\} \tag{2.11}$$

Another consequence of choosing this waveform is that, in the frequency domain, the signal is not bandlimited; however, the amplitude of $W_\beta(f)$ tends to 0 as the frequency

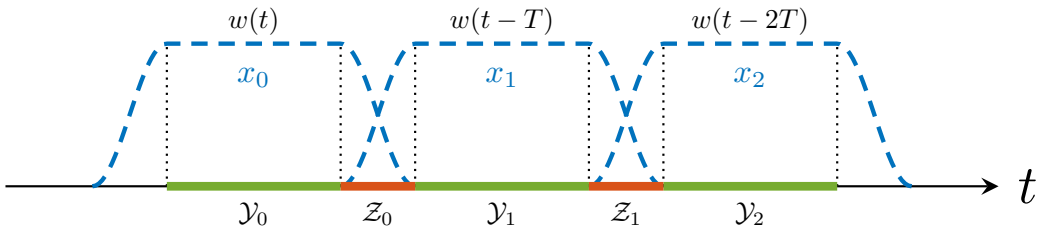

Figure 2.3: ISI-free and ISI-pressent intervals for $n = 3$. Based in [1].

increases, so it is possible to define the bandwidth of the waveform as the smallest interval containing the 95% of the signal energy [1]. With this definition, we get the bandwidths seen in table 2.1 for different β.

β	Bandwith [Hz]	overhead
0.1	1.477	195.4%
0.3	0.788	57.6%
0.5	0.668	33.6%
0.7	0.613	22.6%
0.8	0.592	18.4%
0.9	0.575	15.0%

Table 2.1: Bandwidth containing 95% of the waveform energy, and the overhead compared to the minimum bandwidth for Nyquist signaling. Taken from [1].

2.1.5 Integrate and dump

This block integrates the incoming signal $s(t)$ in the different intervals $\mathcal{Y}_i$ and $\mathcal{Z}_i$ to produce the real valued samples y_i and z_i given by:

$$y_i = \int_{\mathcal{Y}_i} s(t)dt \qquad i \in \{0, \dots, n-1\} \tag{2.12}$$

$$z_i = \int_{\mathcal{Z}_i} s(t)dt \qquad i \in \{0, \dots, n-2\} \tag{2.13}$$

It can be shown that y_i is given by [1]:

$$y_i = \alpha^2(1-\beta)T|x_i|^2 + \alpha|x_i|n_i + m_i \tag{2.14}$$

where $\alpha = 2/\sqrt{4-\beta}$, $n_i \sim \mathcal{N}(0, \sigma_{sh}^2(1-\beta)T)$ and $m_i \sim \mathcal{N}(0, \sigma_{th}^2(1-\beta)T)$.

Also defining:

$$\psi(v, w) = \frac{1}{4}|v+w|^2 + \frac{1}{8}|v-w|^2 \tag{2.15}$$

which can be expanded using equation 1.5 as:

$$\psi(ae^{j\alpha}, be^{j\beta}) = \frac{3}{8}\left(a^2+b^2\right) + \frac{1}{4}ab\cos(\alpha-\beta) \tag{2.16}$$

it is possible to show that z_i is given by [1]:

$$z_i = \alpha^2 \beta T \psi(x_i, x_{i+1}) + \alpha \sqrt{\psi(x_i, x_{i+1})} p_i + q_i \tag{2.17}$$

where $p_i \sim \mathcal{N}(0, \sigma_{sh}^2 \beta T)$ and $q_i \sim \mathcal{N}(0, \sigma_{th}^2 \beta T)$.

Notice that n_i, m_i, p_i, and q_i are mutually independent, and that all the y_i carry information about the magnitude of the transmitted symbols, and all the z_i carry information about the interference between adjacent symbols, i.e., the phase difference between symbols.

2.1.6 Class representative

When transmitting symbol blocks (n consecutive symbols), it turns out that there are some ambiguities, which means that two different symbol blocks produce the same output of the system. Of course, we want to avoid this situation to achieve reliable communication. That is what the Class representative block of figure 2.1 does.

To formalize the problem let define the function $\Upsilon : \mathbb{C}^n \to (\mathbb{R}^n, \mathbb{R}^{n-1})$ that maps a vector $\boldsymbol{x}$ at the input of the signaling block, to the output of the integrate and dump block, in the absence of noise [1]. That means:

$$\Upsilon(\boldsymbol{x}) = (\boldsymbol{y}, \boldsymbol{z}) \tag{2.18}$$

where $\boldsymbol{x} \in \mathbb{C}^n$, $\boldsymbol{y} \in \mathbb{R}^n$, $\boldsymbol{z} \in \mathbb{R}^{n-1}$ and

$$y_i = \int_{\mathcal{Y}_i} \left|x(t)\right|^2 dt \qquad i \in \{0, \ldots, n-1\} \tag{2.19}$$

$$z_i = \int_{\mathcal{Z}_i} \left|x(t)\right|^2 dt \qquad i \in \{0, \ldots, n-2\} \tag{2.20}$$

Now we define an equivalence relation in $\mathbb{C}^n$, where two vectors $\boldsymbol{x}$ and $\tilde{\boldsymbol{x}}$ are square law equivalent if and only if $\Upsilon(\boldsymbol{x}) = \Upsilon(\tilde{\boldsymbol{x}})$, and we denote the equivalence by $\boldsymbol{x} \equiv \tilde{\boldsymbol{x}}$ [1].

The Class representative block consist of a set $\mathcal{S}$ of cardinality M, whose elements belong to $\mathbb{C}^n$ and are all square law distinct [1], that is:

$$\mathcal{S} = \{\boldsymbol{x}_1, \ldots, \boldsymbol{x}_M\} \subset \mathbb{C}^n \qquad \text{such that} \qquad \boldsymbol{x}_i \not\equiv \boldsymbol{x}_l \Leftrightarrow k \neq l \tag{2.21}$$

and for an input $k \in \{1, \ldots, M\}$ the block outputs $\boldsymbol{x}_k$ [1]:

$$k \longrightarrow \boxed{\text{Class Representative}} \longrightarrow \boldsymbol{x}_k \qquad k \in \{1, \ldots, M\} \tag{2.22}$$

Notice that this scheme can transmit M different symbol blocks using n symbols, thus, the spectral efficiency of this channel can not exceed $\frac{1}{n}\log_2(M)$bits/s/Hz [1].

2.1.6.1 Analysis on ambiguities

There are two key points to understand the origin of the ambiguities. The first, and most important, is to notice that the detection of a symbol block is based only on the magnitude

of each symbol (given in each y_i) and the phase difference between adjacent symbols (given in each z_i). That means that every two vectors whose elements have the same magnitude and the phase difference between adjacent elements is the same are square law equivalent.

The second key point is to notice that the symbols of the symbol blocks belong to a constellation $\mathcal{K}$ (some examples of possible constellations are shown in figure 2.8), which means that a $\boldsymbol{x} \in \mathcal{K}^n \subset \mathbb{C}^n$, in other words $\boldsymbol{x}$ belongs to a finite subset of $\mathbb{C}^n$.

In summary, all n-tuple of points in a given constellation with the same magnitudes and phase difference between adjacent symbols are square law equivalent and generate ambiguities. Let us define equivalence class as the set of all such vectors, so an equivalence class $\mathcal{E}$ of size L is given by:

$$\mathcal{E} = \{\boldsymbol{x}_1, \ldots, \boldsymbol{x}_L\} \subset \mathcal{K}^n \qquad \text{such that} \qquad \boldsymbol{x}_i \equiv \boldsymbol{x}_j \quad \forall i, j \in \{1, \ldots, L\} \tag{2.23}$$

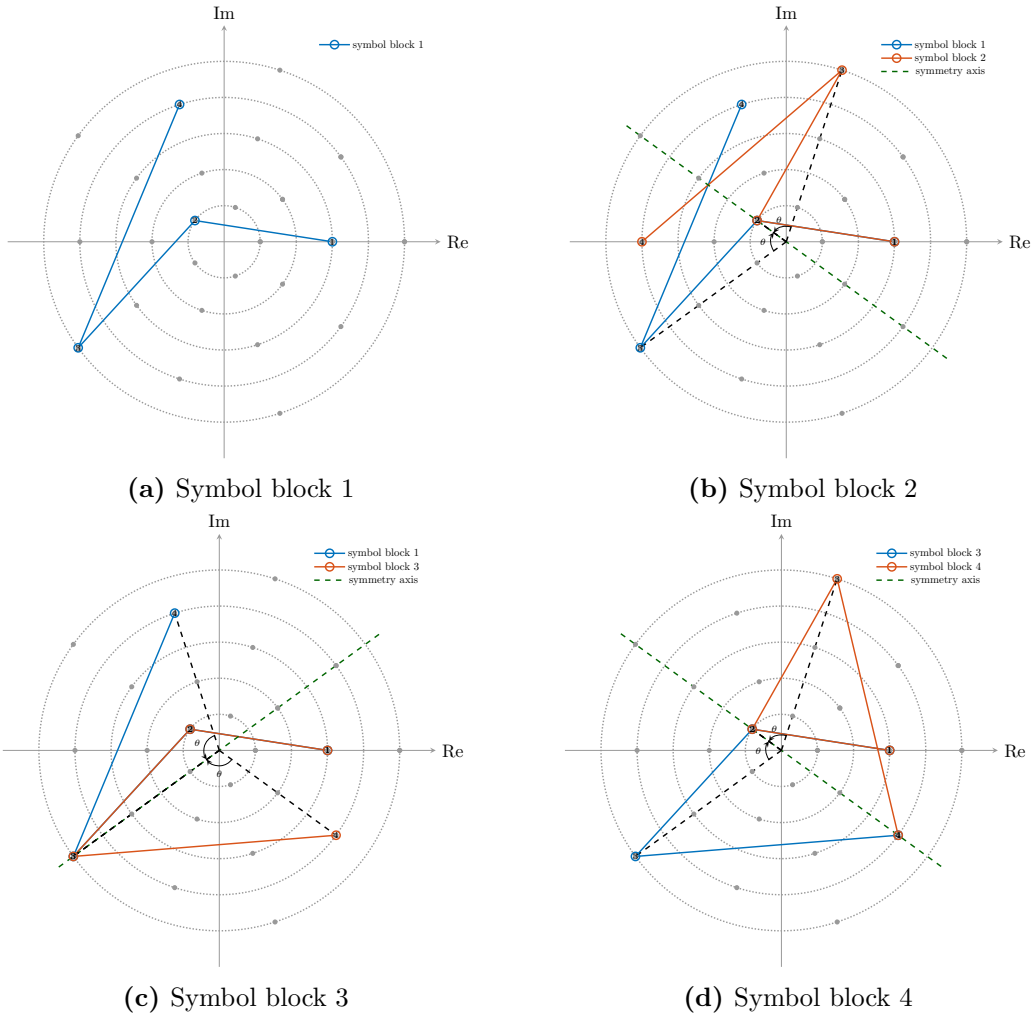

(a) Symbol block 1 **(b)** Symbol block 2

(c) Symbol block 3 **(d)** Symbol block 4

Figure 2.4: Construction of 4 different but square law equivalent symbol blocks.

To understand better the equivalence classes, let us look at an example of an equivalence

class when the symbol block length is $n = 4$, and the constellation is a 5-ring 5-ary phase (see figure 2.8d) and how to construct it.

The first step is to select four random constellation points to create a symbol block. For example, the points shown in figure 2.4a, where the transmitted symbols are the graph's vertices, and the small number in each point gives the transmission order.

To create a new equivalent symbol block, one can reflect the third and fourth symbol along the symmetry axis that passes through the second symbol, as shown in the figure 2.4b. Notice that the first and second symbols do not change; hence, their magnitudes and the phase difference between them are the same. The third and fourth symbols change, but since the symmetry axis passes through the origin, their magnitudes do not change, nor does the phase difference between them. The phase difference between the second and third symbol in both symbol blocks is also the same as shown in figure 2.4b. Finally, all the points of the new symbol block lay on a valid constellation point due to the high symmetry of the constellation. Hence, the first symbol block and the new one are valid (belong to $\mathcal{K}^4$) and square law equivalent, so they belong to the same equivalence class.

The same process can be applied to the fourth symbol, and using as symmetry axis the axis that passes through the third symbol as shown in the figure 2.4c. Using the same arguments, the new symbol block is equivalent to the previous two and belongs to the same equivalence class. From this new symbol block, reflecting the third and fourth symbols as shown in figure 2.4d, one can create a new fourth symbol block belonging to the same equivalence class.

Now, we have four different but square law equivalent symbol blocks. Clearly, if we reflect all four symbols blocks along the real axis, we create four new different symbol blocks that belong to the equivalence class, as shown in figure 2.5.

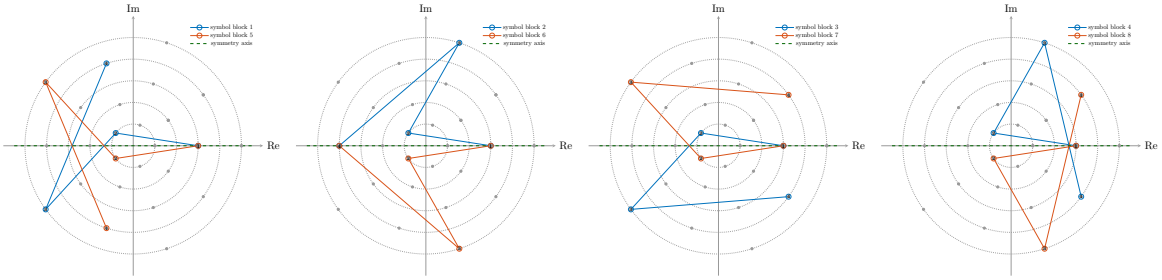

(a) Symbol block 5 **(b)** Symbol block 6 **(c)** Symbol block 7 **(d)** Symbol block 8

Figure 2.5: Construction of 4 new different but square law equivalent symbol blocks by reflection.

Finally, we can rotate all the eight different, but square law equivalent symbol blocks, four times around the origin to create 32 new different symbol blocks that belong to the equivalence class, as shown in figure 2.6. As a result, we get all the symbol blocks that belong to the same equivalence class. Those symbol blocks are shown in figure 2.7.

When looking at all the symbol blocks of the equivalence class (see figure 2.7), it is possible to notice the high symmetry of the plot, this shows that constellations with high symmetry allow a lot of ambiguities and reduce the achievable rate of the system.

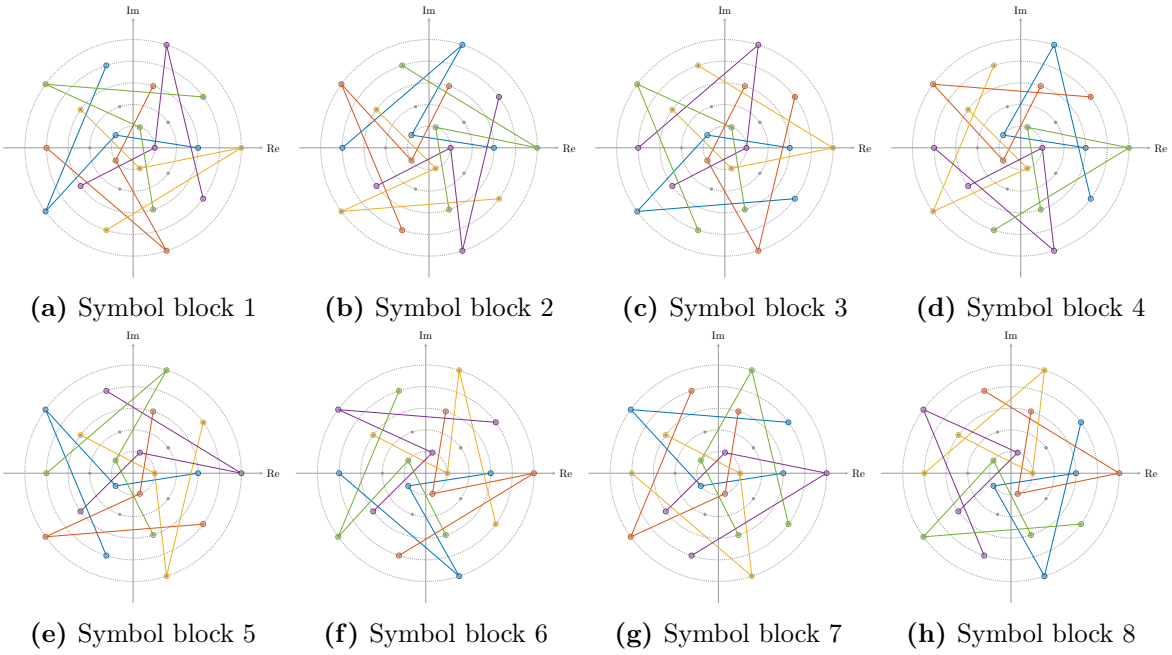

(a) Symbol block 1 **(b)** Symbol block 2 **(c)** Symbol block 3 **(d)** Symbol block 4

(e) Symbol block 5 **(f)** Symbol block 6 **(g)** Symbol block 7 **(h)** Symbol block 8

Figure 2.6: Construction of 32 new different but square law equivalent symbol blocks by rotation.

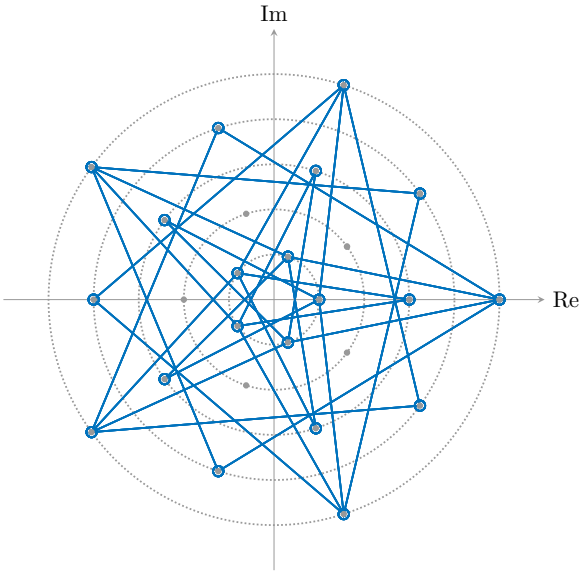

Figure 2.7: All the symbol blocks in an equivalence class shown at the same time.

2.1.7 Detector

For the detection, the maximum-likelihood (ML) criterion is chosen, which means that from $\boldsymbol{y} = (y_0, \ldots, y_{n-1})$ and $\boldsymbol{z} = (z_0, \ldots, z_{n-2})$, the detector outputs $\hat{k}$ if and only if [1]:

$$\hat{k} = \underset{d \in \{1,\ldots,M\}}{\arg\max}\ f\left(\boldsymbol{y}, \boldsymbol{z} | \boldsymbol{x}_d\right) \tag{2.24}$$

Where the PDF of $\boldsymbol{y}, \boldsymbol{z}$ given $\boldsymbol{x}_d$ is given by [1]:

$$f(\boldsymbol{y}, \boldsymbol{z}|\boldsymbol{x}_d) = f(\boldsymbol{y}|\boldsymbol{x}_d) f(\boldsymbol{z}|\boldsymbol{x}_d) = \prod_{i=0}^{n-1} f(y_i|\boldsymbol{x}_d[i]) \prod_{i=0}^{n-2} f(z_i|\boldsymbol{x}_d[i], \boldsymbol{x}_d[i+1]) \tag{2.25}$$

From equations 2.14 and 2.17 it is clear that y_i and z_i given x_i and x_{i+1} are distributed as [1]:

$$y_i \sim \mathcal{N}\left(\alpha^2(1-\beta)T|x_i|^2, (1-\beta)T(\alpha^2|x_i|^2\sigma_{sh}^2 + \sigma_{th}^2)\right) \tag{2.26}$$

$$z_i \sim \mathcal{N}\left(\alpha^2\beta T\psi(x_i, x_{i+1}), \beta T(\alpha^2\psi(x_i, x_{i+1})\sigma_{sh}^2 + \sigma_{th}^2)\right) \tag{2.27}$$

2.2 Numerical simulation

2.2.1 System parameters

For the numerical simulation, the system is simulated in baseband, the baud rate is 10 Gb/s, no attenuation in the optical fiber is considered, and the parameters of the diode are taken from [1] and can be seen on table 2.2.

Parameter	Value	Typical range
Temperature (T)	300 K	
Load resistance (R_L)	15 Ω	
APD Gain (M_{APD})	20	10 - 40
Enhanced Responsivity ($M_{\text{APD}}R_{\text{APD}}$)	10 mA/mW	5 - 20
k-factor (k_{APD})	0.6	0.5 - 0.7
Excess noise factor (F)	12.78	a function of M_{APD} and k_{APD}

Table 2.2: Parameter of the photodiode used in the simulations. Taken from [1].

2.2.2 Class representative creation

To define the Class representative block, one must specify a constellation and a block length n, then look for all the equivalence classes exhaustively, and finally select one random symbol block from each equivalence class to conform the class representative. In this step, several constellations are considered with different block lengths; six examples of constellations are shown in figure 2.8.

To calculate those equivalence classes, we use a Python script that is available on the GitHub repository Direct_detection_under_Tukey_Signaling, all the related codes are in the folder **Equivalence_classes**. We get all the equivalence classes for the studied constellations and block length from this code. The summary can be seen in the tables 2.3 to 2.6 that show the number of equivalence classes sorted by the class size L and the total of equivalence classes for different block lengths n, finally is also shown the rate loss, calculated as:

$$R_{\text{loss}} = \frac{1}{n}\log_2\left(\frac{|\mathcal{K}|^n}{N_{\text{Eq class}}}\right) \tag{2.28}$$

where $|\mathcal{K}|$ denotes the number of points of the constellation, and $N_{\text{Eq class}}$ the total of equivalence classes.

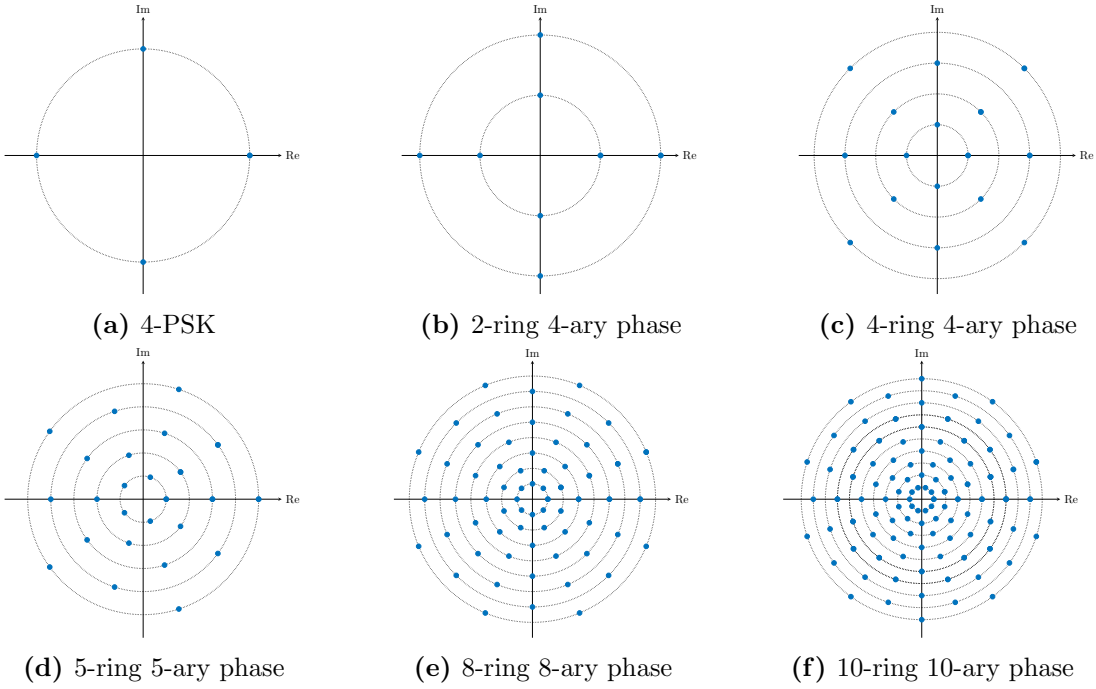

(a) 4-PSK **(b)** 2-ring 4-ary phase **(c)** 4-ring 4-ary phase

(d) 5-ring 5-ary phase **(e)** 8-ring 8-ary phase **(f)** 10-ring 10-ary phase

Figure 2.8: Different possible constellations $\mathcal{K}$.

Class size \ Block length	3	4	5	6	7	8
4	4	8	16	32	64	128
8	4	12	32	80	192	448
16	1	6	24	80	240	672
32		1	8	40	160	560
64			1	10	60	280
128				1	12	84
256					1	14
512						1
Total	9	27	81	243	729	2187
Rate loss (bit/sym)	0.94	0.81	0.73	0.68	0.64	0.61

Table 2.3: Number of equivalence classes for 4-PSK constellation.

2.2.3 Mutual information estimation

One of the figures of merit of the system is the Mutual information (MI) I of the channel, which is given by [8]:

$$I = \sum_{x,y} P(x,y) \log_2 \left(\frac{P(x,y)}{P(x)P(y)} \right) \tag{2.29}$$

To estimate the mutual information we use a Python script to implement a Montecarlo simulation with 100 000 symbol blocks (code available on the GitHub repository Direct_detection_under_Tukey_Signaling, in the folder **skripts** file **main.py**). In this case, all

Class size \ Block length	3	4	5	6	7
4	32	128	512	2048	8192
8	32	192	1024	5120	24576
16	8	96	768	5120	30720
32		16	256	2560	20480
64			32	640	7680
128				64	1536
256					128
Total	72	432	2592	15552	93312
Rate loss (bit/sym)	0.94	0.81	0.73	0.68	0.64

Table 2.4: Number of equivalence classes for 2-ring 4-ary Phase constellation.

Class size \ Block length	3	4
5	125	625
10	500	3750
20	500	7500
40		5000
Total	1125	16875
Rate loss (bit/sym)	1.27	1.13

Table 2.5: Number of equivalence classes for 5-ring 5-ary Phase constellation.

Class size \ Block length	3
8	512
16	3584
32	6272
Total	10368
Rate loss (bit/sym)	1.55

(a) 8-ring 8-ary Phase

Class size \ Block length	3
10	100
20	9000
40	20250
Total	30250
Rate loss (bit/sym)	1.68

(b) 10-ring 10-ary Phase

Table 2.6: Number of equivalence classes for different constellations.

the possible square law distinct symbol blocks are used for the simulation.

For the 2-ring 4-ary phase constellation and symbol block length $n = 3$, we simulated for four different β and got the results shown in figure 2.9. Notice that for medium and high SNR, the best choice of beta is $\beta = 0.9$; also is important to observe that the mutual information tends to 2.06 bit/sym approximately, which is coherent with the rate loss calculated (see table 2.4)

$$2.06\,\text{bit/sym} = 3\,\text{bit/sym} - 0.94\,\text{bit/sym}$$

Also, it is important to notice that the obtained results are coherent with the results reported by [1], which shows that the implementation of the system we made is well done.

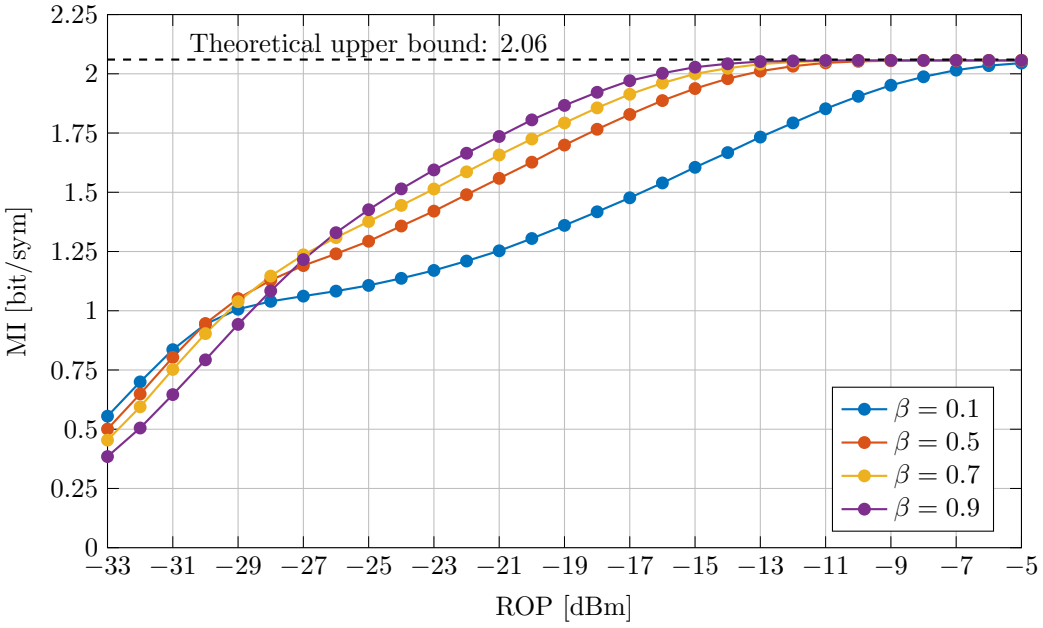

Figure 2.9: Mutual information of the system with 2-ring 4-ary phase constellation and symbol block length $n = 3$.

2.2.4 BER estimation

Once again, a Montecarlo simulation is used to estimate the BER, but this time, not all the square law distinct symbols are used. Instead, we use the biggest power of two [1]. For example, for the 2-ring 4-ary phase constellation and symbol block length $n = 4$, we use 256 square law distinct symbol blocks instead of 432.

Again, we simulated for different β, the 2-ring 4-ary phase constellation, and symbol block length $n = 4$ to get the results shown in figure 2.10. The results show the typical behavior of a BER vs SNR graph. Again, the case of $\beta = 0.9$ has the best performance, and the results are coherent with the ones presented by [1].

2.3 Discussion

After implementing the system of Tukey signaling, we noticed that the system, at least in simulation and an ideal situation, should work well and be able to retrieve some information about the phase of the complex symbols using only DD. However, the system has three downsides: the complexity of the decoder, the bandwidth efficiency, and the implementation.

To decrease the rate loss in this system, one can increase the block length, but the number of equivalence classes grows exponentially with the block length, and so does the complexity of the decoder. That is why the system becomes impractical really quickly, which shows that the complexity of the decoder is a big drawback of the system.

Another drawback is the bandwidth efficiency; since the Tukey signal is time-limited, its bandwidth is, in theory, unlimited and, in practice, really big compared to other waveforms,

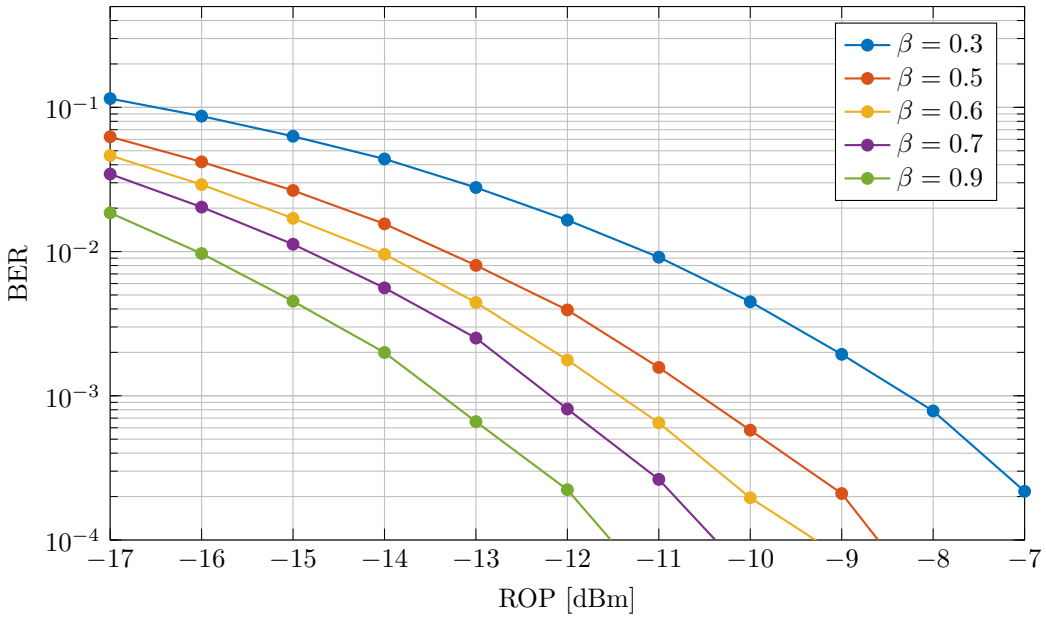

Figure 2.10: Bit error rate of the system with 2-ring 4-ary phase constellation and symbol block length $n = 4$.

such as a sinc pulse. To solve this problem, one should increase the duration of the pulse, but by doing so, the idea of the integrate and dump block is no longer valid because, at some points in time, more than two symbols may influence the signal, and the idea of the system was based on the assumption that at any time at most two symbols influence the signal.

Finally, the integrate and dump is an analog block by default, which may be complicated to implement, and a digital approximation of the block requires a big oversampling factor, which is too expensive in terms of the hardware to implement.

We decided to look for other solutions in the literature for these three drawbacks and stop the work with the system proposed by Tasbihi in [1].

This page intentionally left blank.

Chapter 3

Generalized Direct Detection with phase recovery

The other solution considered for the phase recovery problem is the one proposed by Plabst in the paper [7]. The authors try to improve the two drawbacks of the Tukey signaling scheme. First, they considered an arbitrary pulse waveform, and in particular, they experimented with raised cosine waveforms to improve the spectral efficiency. Second, they propose a discrete-time model, which allows the use of a digital system with an oversampling factor of only two.

The proposed system model can be seen in figure 3.1. In the following sections, we will explain the system model, both in continuous and discrete time, and the detector used to determine an upper bound limit of the system's performance.

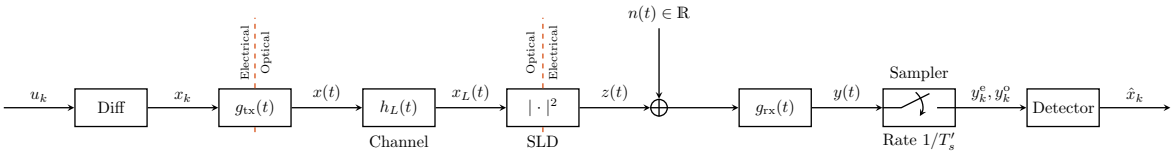

Figure 3.1: System model proposed in [7].

3.1 System model

3.1.1 Continuous time Model

3.1.1.1 Differential encoder

As it was mentioned in chapter 2 the DD generates some ambiguities, and one way to eliminate them is by using differential encoding [6], [7], [9]. As suggested in [9], the phase encoding is done by a function that receives as an input a vector of symbols $\boldsymbol{u}$ and outputs

a vector of symbols $\boldsymbol{x} = f_{\text{diff}}(\boldsymbol{u})$ with the same magnitude as the symbols in $\boldsymbol{u}$, and a given phase based on a set of conditions, the phase of the input symbol and the phase of the last output symbol, as shown for example in figure 3.2 for a M-ASK constellation.

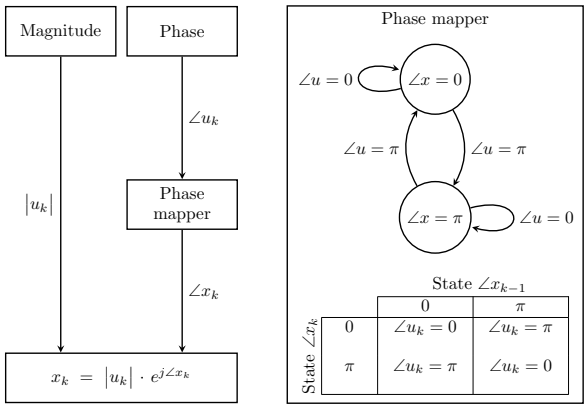

Figure 3.2: Differential phase mapper example for M-ASK. Based on [9].

3.1.1.2 Transmitter

The transmitter receives as input a sequence $\boldsymbol{x} = \{x_0, \ldots, x_{n-1}\}$ of independent and identically distributed (i.i.d.) symbols x_i taken from a finite constellation $\mathcal{K} = \{a_1, \ldots, a_q\}$ with q elements, and outputs a signal given by [7]:

$$x(t) = \sum_{k=0}^{n-1} x_k \cdot g_{\text{tx}}(t - iT) \tag{3.1}$$

where T is the inverse of the symbol rate, $x_i \in \mathcal{K}$, and $g_{\text{tx}}(t)$ is the pulse waveform.

Common pulse waveforms are raised cosine pulses. Of particular interest is the case for roll-off factor $\alpha = 0$, that is:

$$g_{\text{tx}} = \frac{t}{T_s}\text{sinc}\left(\frac{1}{T_s}\right) \tag{3.2}$$

$$G_{\text{tx}} = \begin{cases} 1 & \text{if } |f| \leq \frac{1}{2T_s} \\ 0 & \text{otherwise} \end{cases} \tag{3.3}$$

3.1.1.3 Fiber Optic Link

The channel considered is an optic fiber that only presents chromatic dispersion, characterized in the frequency domain by [7]:

$$H_L(f) = e^{j2\beta_2 L\pi^2 f^2} \tag{3.4}$$

where β_2 is the group-velocity dispersion parameter and L is the fiber length.

3.1.1.4 Receiver

The receiver consists of a photodiode, whose output is given by:

$$z(t) = |x_L(t)|^2 \tag{3.5}$$

The photodiode noise is modeled as a real-valued white Gaussian process with spectral density $N_0/2$ [7], representing the thermal noise. Finally, the receiver has a band-limited sampler, with an impulse response given by:

$$g_{\text{rx}} = 2B\text{sinc}\left(2Bt\right) \tag{3.6}$$

$$G_{\text{rx}} = \begin{cases} 1 & \text{if } |f| \leq B \\ 0 & \text{otherwise} \end{cases} \tag{3.7}$$

where B is the symbol rate given by $B = 1/T_s$ [7].

3.1.2 Discrete time Model

3.1.2.1 Discrete signal notation

For the discrete-time model, a receiver with sampling rate $1/T_s' = 2B$ is considered (in this section, the super index $'$ denotes a variable of the oversampled system), that is an oversampling factor of $N_{\text{os}} = T_s/T_s' = 2$, meaning two samples per transmitted symbol [7].

Let $\boldsymbol{x}' = \{0, x_0, \ldots 0, x_{n-1}\}$ and $\boldsymbol{y}' = \{y_0, \ldots, y_{2n-1}\}$ be the upsampled sequence at the transmitter and receiver, so they are related by [7]:

$$y_k' = z_k' + n_k' \tag{3.8}$$

$$z_k' = \left(|x_L(t)|^2 * g_{\text{rx}}(t)\right)_{t=kT_s'} \tag{3.9}$$

where $n_k \sim \mathcal{N}(0, \sigma_N^2)$ and $\sigma_N^2 = N_0 B$.

Now let us define the combined impulse response of the pulse shaping filter and the channel response as $\psi(t) = g_{\text{tx}}(t) * h_L(t)$ and the discrete version of it $\psi_k = \psi(kT_s')$, then [7]:

$$x_L(kT_s') = \sum_{m=0}^{2n-1} \psi_m x_{k-m}' \tag{3.10}$$

Finally, notice that, for the special case when the pulse shape is the sinc pulse in equations 3.2 and 3.3, $|x_L(t)|^2 * g_{\text{rx}} = |x_L(t)|^2$, so:

$$z_k' = \left| \sum_{m=0}^{2n-1} \psi_m x_{k-m}' \right|^2 \tag{3.11}$$

3.1.2.2 Vector matrix notation

Now, if we think of the signals as column vectors:

$$\begin{aligned} \boldsymbol{x}' &= \left[0, x_0, \ldots, 0, x_{n-1}\right]^T && \in \mathbb{C}^{2n\times 1} \\ \boldsymbol{z}' &= \left[z_0, \ldots, z_{2n-1}\right]^T && \in \mathbb{R}^{2n\times 1} \\ \boldsymbol{n}' &= \left[n_0, \ldots, n_{2n-1}\right]^T && \in \mathbb{R}^{2n\times 1} \\ \boldsymbol{y}' &= \left[y_0, \ldots, y_{2n-1}\right]^T && \in \mathbb{R}^{2n\times 1} \end{aligned}$$

And consider that ψ is time limited, so ψ_m is zero outside some interval $[0, M-1]$, let us define the Toeplitz matrix $\boldsymbol{\Psi} \in \mathbb{C}^{2n\times(2n+M-1)}$ as:

$$\boldsymbol{\Psi} = \begin{bmatrix} \psi_{M-1} & \psi_{M-2} & \cdots & \psi_0 & & & & \\ & \psi_{M-1} & \cdots & \psi_1 & \psi_0 & & & \\ & & \ddots & & & \ddots & & 0 \\ & & & \psi_{M-1} & \cdots & \cdots & \psi_0 & \\ & 0 & & & \ddots & & & \ddots \\ & & & & & \psi_{M-1} & \cdots & \cdots & \psi_0 \end{bmatrix} \tag{3.12}$$

Finally define the channel state $\boldsymbol{s}_0$ as:

$$\boldsymbol{s}_0' = [0, x_{-\widetilde{M}}, 0, x_{1-\widetilde{M}}, \ldots, 0, x_{-1}]^T \in \mathbb{C}^{(M-1)\times 1} \tag{3.13}$$

where $\widetilde{M}$ is the memory channel in terms of the transmitted symbols and is given by $\widetilde{M} = (M-1)/2$.

With the previous definitions, the output of the square law detection is given by:

$$\boldsymbol{z}' = \left| \boldsymbol{\Psi} \begin{bmatrix} \boldsymbol{s}_0' \\ \boldsymbol{x}' \end{bmatrix} \right|^{\circ 2} = \left| \boldsymbol{\Psi} \tilde{\boldsymbol{x}'} \right|^{\circ 2} \qquad \in \mathbb{R}^{2n}$$

where $|\cdot|^{\circ 2}$ is the element wise $|\cdot|^2$ operator.

Finally, the complete discrete-time system model, including the Gaussian noise, is given by [7]:

$$\boldsymbol{y}' = \boldsymbol{z}' + \boldsymbol{n}' = \left| \boldsymbol{\Psi} \tilde{\boldsymbol{x}'} \right|^{\circ 2} + \boldsymbol{n}' \qquad \in \mathbb{R}^{2n}$$

and the channel's conditional probability density is Gaussian[7]:

$$p(\boldsymbol{y}'|\boldsymbol{x}') = \mathcal{N}\left(\boldsymbol{y} - \left| \boldsymbol{\Psi} \tilde{\boldsymbol{x}'} \right|^{\circ 2} ; \boldsymbol{0}_{2n}, \sigma_N^2 \boldsymbol{I}_{2n} \right) \tag{3.14}$$

3.1.2.3 Even and odd samples

For convenience one can concatenate the k-th and $(k+1)$-th sample in a new vector as follows:

$$\boldsymbol{z}_k = \left[z_{2k}', z_{2k+1}' \right] = \left[z_k^{\mathrm{e}}, z_k^{\mathrm{o}} \right] \tag{3.15}$$

$$\boldsymbol{y}_k = \left[y_k^{\mathrm{e}}, y_k^{\mathrm{o}} \right] = \boldsymbol{z}_k + \left[n_k^{\mathrm{e}}, n_k^{\mathrm{o}} \right] \tag{3.16}$$

The reason for group two samples can be understood by looking at the figure 3.3. The convolution and the SQL detection are represented for an even and odd sample in the case of link length $L = 0$. For this choice of waveform, the even sample is an ISI-free sample and carries information about the magnitude of a past symbol; in contrast, the odd sample experiences ISI and, hence, somehow has information about the phases of the symbols.

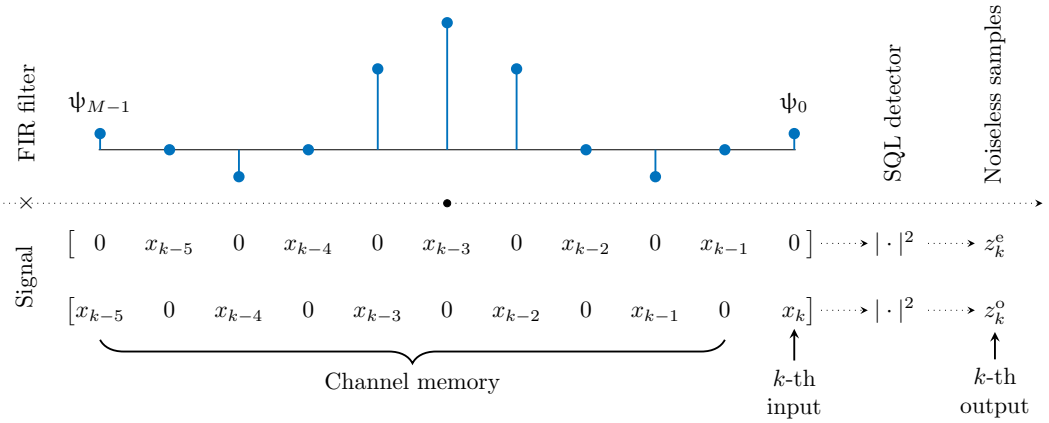

Figure 3.3: Signals for oversampling factor $N_{\mathrm{os}} = 2$. Based on [7].

3.1.3 Symbol-wise MAP detection

To evaluate the optimal performance of the system, in [7] is proposed a decoder based on the maximum a posteriori rule that decides the transmitted symbol based on the a posteriori probabilities (APP) $p(x_k|\boldsymbol{y}')$. Since the APPs are proportional to $p(x_k, \boldsymbol{y}')$ because $p(\boldsymbol{y}')$ is constant with respect to the decision, the MAP rule becomes [7]:

$$\hat{x}_k = \arg\max_{x_k} p(x_k, \boldsymbol{y}') \tag{3.17}$$

as a reminder, $\boldsymbol{y}'$ is the hole vector of received samples, i.e. $\boldsymbol{y}' = \left[y_0, \ldots, y_{2n-1}\right]^T$, and $p(x_k, \boldsymbol{y}')$ is given by [7]:

$$p(x_k, \boldsymbol{y}') = \sum_{s_0} \sum_{\boldsymbol{x}\setminus x_k} p(s_0, \boldsymbol{x}, \boldsymbol{y}') \tag{3.18}$$

and $\sum_{\boldsymbol{x}\setminus x_k}$ denotes a sum over all possible vectors $\boldsymbol{x}$ but where the k-th position is fixed.

These APPs can be efficiently computed with the Forward-Backward Algorithm or BCJR algorithm with the factor graph shown in figure 3.4 and the following recursive equations [7]:

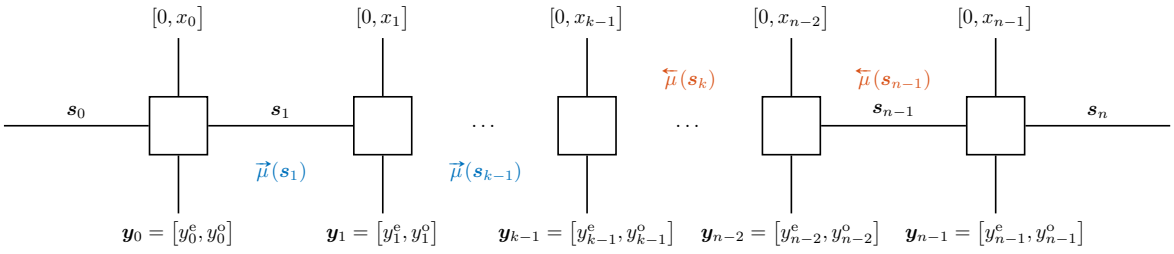

Figure 3.4: Factor graph to implement the BCJR. Based on [7].

$$\overrightarrow{\mu}(\boldsymbol{s}_k) = \sum_{x_k, \boldsymbol{s}_{k-1}} p(x_k, \boldsymbol{y}_k, \boldsymbol{s}_k | \boldsymbol{s}_{k-1}) \cdot \overrightarrow{\mu}(\boldsymbol{s}_{k-1}) \qquad \text{FW path} \tag{3.19}$$

$$\overleftarrow{\mu}(\boldsymbol{s}_{k-1}) = \sum_{x_k, \boldsymbol{s}_k} p(x_k, \boldsymbol{y}_k, \boldsymbol{s}_k | \boldsymbol{s}_{k-1}) \cdot \overleftarrow{\mu}(\boldsymbol{s}_k) \qquad \text{BW path} \tag{3.20}$$

$$p(x_k, \boldsymbol{y}') = \sum_{\boldsymbol{s}_{k-1}} \sum_{\boldsymbol{s}_k} \overrightarrow{\mu}(\boldsymbol{s}_{k-1}) \cdot p(x_k, \boldsymbol{y}_k, \boldsymbol{s}_k | \boldsymbol{s}_{k-1}) \cdot \overleftarrow{\mu}(\boldsymbol{s}_k) \qquad \text{APP} \tag{3.21}$$

where $k = 1, \ldots, n$, $\overrightarrow{\mu}(\boldsymbol{s}_0) = p(\boldsymbol{s}_0)$ and $\overleftarrow{\mu}(\boldsymbol{s}_n) = p(\boldsymbol{s}_n)$.

Finally, the likelihood is given by [7]:

$$p(x_k, \boldsymbol{y}_k, s_k | \boldsymbol{s}_{k-1}) = \underbrace{p(\boldsymbol{y}_k | x_k, \boldsymbol{s}_{k-1})}_{(a)} \underbrace{p(\boldsymbol{s}_k | x_k, \boldsymbol{s}_{k-1})}_{(b)} \underbrace{p(x_k | \boldsymbol{s}_{k-1})}_{(c)} \tag{3.22}$$

where (a) is:

$$p(\boldsymbol{y}_k | x_k, \boldsymbol{s}_{k-1}) = p(y_k^{\mathrm{e}} | \boldsymbol{s}_{k-1}) \cdot p(y_k^{\mathrm{o}} | x_k, \boldsymbol{s}_{k-1}) \tag{3.23}$$

$$p(y_k^{\mathrm{e}} | \boldsymbol{s}_{k-1}) = p_N \left(y_k^{\mathrm{e}} - \left| [0, x_{k-\widetilde{M}}, \cdots, 0, x_{k-1}, 0] \cdot \psi \right|^2 \right) \tag{3.24}$$

$$p(y_k^{\mathrm{o}} | x_k, \boldsymbol{s}_{k-1}) = p_N \left(y_k^{\mathrm{o}} - \left| [x_{k-\widetilde{M}}, 0, \cdots, x_{k-1}, 0, x_k] \cdot \psi \right|^2 \right) \tag{3.25}$$

The term (b) is 1 if the state transition from $\boldsymbol{s}_{k-1}$ to $\boldsymbol{s}_k$ is possible and 0 otherwise, and (c) is $p(x_k | \boldsymbol{s}_{k-1}) = p(x_k)$ since the symbols are i.i.d. [7].

Additionally, since using differential encoding is recommended to avoid ambiguities, one can include the differential decoding in the BCJR algorithm by including the fact that $\boldsymbol{x} = f_{\mathrm{diff}}(\boldsymbol{u})$ in the factor graph [7]. That is done by doing the summations in equations 3.19, 3.20 and 3.21 overall u_k instead of x_k (which in terms of the algorithm makes no change), and defining the states of equations 3.24 and 3.25 in terms of the $\boldsymbol{u}$, that means replacing $\boldsymbol{x}$ by $f_{\mathrm{diff}}(\boldsymbol{u})$ (for more details see the algorithm used in [10]).

3.2 Numerical simulation

For the numerical simulations we implemented the proposed system model in a Python simulation, which can be found in the git repository Direct_Detection_with_Phase_Recovery. As the system parameters we use the settings found in table 3.1, and we estimate the SER using a Montecarlo simulation with 20 000 transmitted symbols. We set the noise power to $\sigma_N^2 = 1$ so the SNR is given by [7]:

$$\mathrm{SNR} = P_{\mathrm{tx}} = \frac{\mathbb{E}\big[||x(t)||\big]}{nT_s} \tag{3.26}$$

For the pulse shaping filter, we used a sinc pulse with a sampling rate of $2B$. Since the complexity of the decoder grows exponentially with the length of the filter, we could not use

Paramater	Value
β_2	$-2.168 \times 10^{-23}\,\mathrm{s}^2/\mathrm{km}$
attenuation factor	$0.2\,\mathrm{dB/km}$
link lengths L	$0\,\mathrm{km}$
Baud rate B	$35\,\mathrm{Gbaud}$

Table 3.1: Simulation parameters. Taken from [7].

in the decoder the complete signal $\psi(t)$, instead of that we use an auxiliary channel for the decoding process that considers only a window of the real channel as shown in figure 3.5. That means, we simulated the transmission with a channel with memory (in terms of the transmitted symbols) of $\widetilde{M}$, i.e. $M = 2\widetilde{M} + 1$ taps, but decode with an auxiliary channel with memory $\widetilde{N}$ i.e. $N = 2\widetilde{N} + 1$ taps.

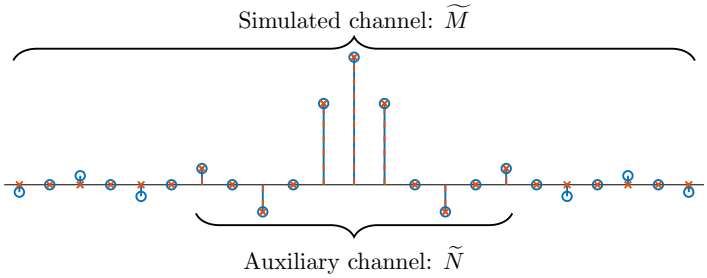

Figure 3.5: Simulated and auxiliary channel. Based on [7].

For the constellations, we choose three different constellations, BPSK, 4-QAM, and DD-SQAM, a specially designed constellation, shown in figure 3.6, to mitigate the ambiguities that arise from the DD. As pointed out in section 2.1.6.1, constellations with high symmetry produce a lot of ambiguities, and the DD process only distinguishes the phase difference between symbols through the cosine of the phase difference, so when designing the DD-SQAM constellation, we reduced the symmetry, and separate the cosine of the angle between symbols as much as possible, that is why we use the particular angle $\phi = \arccos(1/3)$.

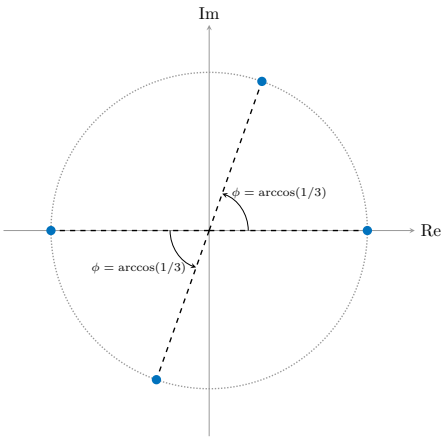

Figure 3.6: DD-SQAM constellation.

Finally, we simulate two scenarios for each constellation, one when the auxiliary channel is much shorter than the actual channel and the other when the auxiliary and the actual channels have the same length. The length of the auxiliary channel is chosen based on complexity criteria; we choose a relatively large length that is still computable in a reasonable time. The results can be seen in figure 3.7.

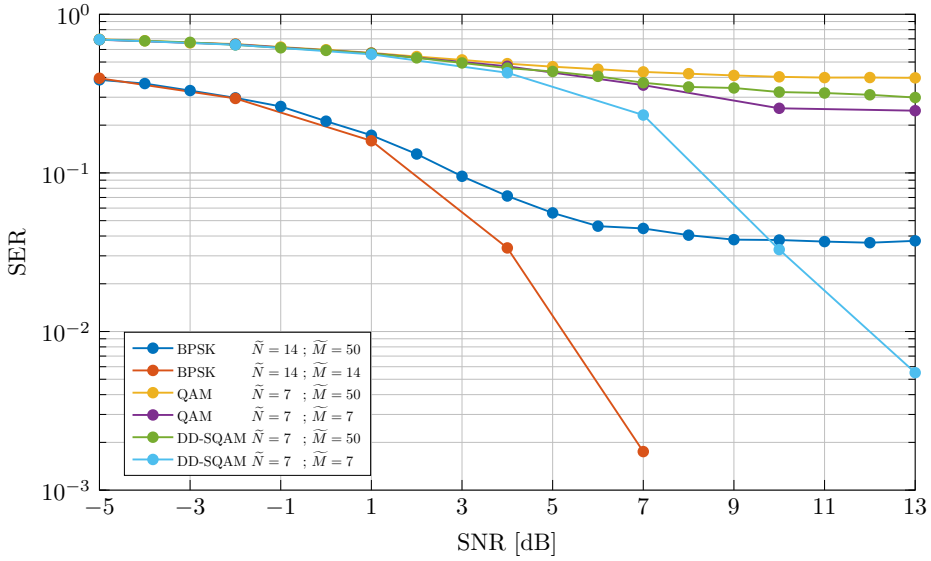

Figure 3.7: Symbol error rate vs SNR for different constellations and channel lengths.

Looking at the figure 3.7, we can notice that the simulations with a channel miss-match ($\widetilde{N} < \widetilde{M}$) have an error floor, this is due to the ISI that is not considered by the BCJR decoder, so even increasing the SNR, the SER does not improve, because the main source of "noise" is the ISI.

It is also important to notice that the QAM constellation with $\widetilde{N} = \widetilde{M}$ also has an error floor at approximately 0.25; this is caused by the ambiguities generated by the DD for the case of the QAM constellation. Even with differential encoding, there are still ambiguities 1/4 of the time because a phase change of π or 0 can be distinguished, but a phase change of $\pm\pi/2$ can not. Finally, it is important to notice that the BPSK and DD-SQAM constellations do not have an error floor when $\widetilde{N} = \widetilde{M}$. This shows that these constellations do not generate ambiguities when used with differential encoding.

3.3 Discussion

The system proposed in [7] compared with the system proposed in [1] has the advantage of using a waveform with a smaller bandwidth that increases the spectral efficiency [7], and also represents a simpler system compatible with a digital system with an oversampling factor of only 2, which is very desirable. However, the problem of finding a good decoder with feasible complexity is still open.

For this reason, we use this system as a base to formulate a machine learning-based decoder, which will be discussed in the next chapter.

Chapter 4

MagPhase-DetNet

We try to implement a decoder based on the DetNet decoder proposed in [11], [12]. There, the authors propose a machine learning-based architecture for a MIMO AWGN linear channel. In those papers, the authors noticed that the detection problem is equivalent to the following minimization problem in the MIMO case [11]:

$$\hat{\boldsymbol{x}} = \arg \min_{\boldsymbol{x} \in \mathcal{K}^n} \|\boldsymbol{y} - \boldsymbol{H}\boldsymbol{x}\|^2 \tag{4.1}$$

Hence, it may be solved by gradient descent. However, the solution found by gradient descent could be invalid because the vector $\hat{\boldsymbol{x}}$ may not belong to $\mathcal{K}^n$. That is why the authors propose a projected gradient descent, where in every iteration, the new estimated vector is somehow projected in $\mathcal{K}^n$. With this in mind, the authors in [11], [12] proposed to unfold the iterations of the gradient descent and perform each iteration with a layer of a neural network, and at the end have an estimation of the vector $\hat{\boldsymbol{x}}$.

As reported in [11], [12], the performance of the architecture is as gut as the state-of-the-art decoders, but at least 30 times faster, which makes the architecture promising.

The reason for trying this architecture is the similitude of the MIMO problem (equation 4.1) and the DD problem:

$$\hat{\tilde{\boldsymbol{x}}}' = \arg \min_{\tilde{\boldsymbol{x}}' \in \mathbb{K}^{2n}} \left\| \boldsymbol{y} - \left| \boldsymbol{\Psi} \tilde{\boldsymbol{x}}' \right|^{\circ 2} \right\|^2 \tag{4.2}$$

where the main difference is the non linear $|\cdot|^{\circ 2}$ operator. Which does not impede the implementation of the DetNet architecture.

In the following sections, we will follow the steps in [12] to propose an architecture for the DD problem based on the system model presented in chapter 3, and give some numerical simulation results.

4.1 Separation in even and odd subchannel

The first thing we do to cast the problem for the DetNet architecture is to separate the hole system into two subchannels. For doing so, we take advantage of the oversampling factor of 2 and distinction of even and odd samples done in equations 3.15 and 3.16.

For doing that we started from the not upsampled $\boldsymbol{x}$ and $\boldsymbol{s}_0$ vector:

$$\boldsymbol{x} = \begin{bmatrix} x_0 & x_1 & \cdots & x_{n-1} \end{bmatrix}^T \qquad \in \mathbb{C}^n \tag{4.3}$$

$$\boldsymbol{s}_0 = \begin{bmatrix} x_{-\widetilde{M}} & x_{1-\widetilde{M}} & \cdots & x_{-1} \end{bmatrix}^T \qquad \in \mathbb{C}^{\widetilde{M}} \tag{4.4}$$

$$\tilde{x} = \begin{bmatrix} \boldsymbol{s}_0 & \boldsymbol{x} \end{bmatrix}^T \qquad \in \mathbb{C}^{n+\widetilde{M}} \tag{4.5}$$

and define the following subchannel matrices:

$$\boldsymbol{\Psi}_{\mathrm{o}} = \begin{bmatrix} \psi_{M-1} & \psi_{M-3} & \cdots & \psi_0 & & & & & \\ & \psi_{M-1} & \cdots & \psi_2 & \psi_0 & & & & \\ & & \ddots & & & \ddots & & 0 & \\ & & & \psi_{M-1} & \cdots & \cdots & \psi_0 & & \\ & 0 & & & \ddots & & & \ddots & \\ & & & & & \psi_{M-1} & \cdots & \cdots & \psi_0 \end{bmatrix} \qquad \in \mathbb{C}^{n\times(n+\widetilde{M})} \tag{4.6}$$

$$\boldsymbol{\Psi}_{\mathrm{e}} = \begin{bmatrix} \psi_{M-2} & \psi_{M-4} & \cdots & \psi_1 & 0 & & & & & \\ & \psi_{M-2} & \cdots & \psi_3 & \psi_1 & 0 & & & & \\ & & \ddots & & & \ddots & \ddots & 0 & & \\ & & & \psi_{M-2} & \cdots & \cdots & \psi_1 & 0 & & \\ & 0 & & & \ddots & & & \ddots & \ddots & \\ & & & & & \psi_{M-2} & \cdots & \cdots & \psi_1 & 0 \end{bmatrix} \qquad \in \mathbb{C}^{n\times(n+\widetilde{M})} \tag{4.7}$$

with these definitions, the problem transforms into:

$$\begin{bmatrix} \boldsymbol{y}_{\mathrm{e}} & \boldsymbol{y}_{\mathrm{o}} \end{bmatrix} = \begin{bmatrix} \boldsymbol{z}_{\mathrm{e}} & \boldsymbol{z}_{\mathrm{o}} \end{bmatrix} + \begin{bmatrix} \boldsymbol{n}_{\mathrm{e}} & \boldsymbol{n}_{\mathrm{o}} \end{bmatrix} \tag{4.8}$$

$$= \begin{bmatrix} |\boldsymbol{\Psi}_{\mathrm{e}}\tilde{\boldsymbol{x}}|^{\circ 2} & |\boldsymbol{\Psi}_{\mathrm{o}}\tilde{\boldsymbol{x}}|^{\circ 2} \end{bmatrix} + \begin{bmatrix} \boldsymbol{n}_{\mathrm{e}} & \boldsymbol{n}_{\mathrm{o}} \end{bmatrix} \tag{4.9}$$

$$\tag{4.10}$$

which can be separated into two independent and fictitious channels:

$$\boldsymbol{y}_{\mathrm{e}} = \boldsymbol{z}_{\mathrm{e}} + \boldsymbol{n}_{\mathrm{e}} = |\boldsymbol{\Psi}_{\mathrm{e}}\tilde{\boldsymbol{x}}|^{\circ 2} + \boldsymbol{n}_{\mathrm{e}} \qquad \in \mathbb{R}^n \tag{4.11}$$

$$\boldsymbol{y}_{\mathrm{o}} = \boldsymbol{z}_{\mathrm{o}} + \boldsymbol{n}_{\mathrm{o}} = |\boldsymbol{\Psi}_{\mathrm{o}}\tilde{\boldsymbol{x}}|^{\circ 2} + \boldsymbol{n}_{\mathrm{o}} \qquad \in \mathbb{R}^n \tag{4.12}$$

4.2 Real and imaginary reparametrization

To be able to work with the Pytorch framework, we cast the original problem, which has complex numbers, in one problem that is completely real. For doing that, we redefine $\boldsymbol{\Psi}_{\mathrm{e,ML}}$,

$\boldsymbol{\Psi}_{\text{o,ML}}$ and $\tilde{\boldsymbol{x}}_{\text{ML}}$ as suggested in [12] (where the subindex "ML" stands for machine learning):

$$\boldsymbol{\Psi}_{\text{e,ML}} = \begin{bmatrix} \text{Re}\{\boldsymbol{\Psi}_{\text{e}}\} & -\text{Im}\{\boldsymbol{\Psi}_{\text{e}}\} \\ \text{Im}\{\boldsymbol{\Psi}_{\text{e}}\} & \text{Re}\{\boldsymbol{\Psi}_{\text{e}}\} \end{bmatrix} \qquad \in \mathbb{R}^{2n \times 2(n+\widetilde{M})} \tag{4.13}$$

$$\boldsymbol{\Psi}_{\text{o,ML}} = \begin{bmatrix} \text{Re}\{\boldsymbol{\Psi}_{\text{o}}\} & -\text{Im}\{\boldsymbol{\Psi}_{\text{o}}\} \\ \text{Im}\{\boldsymbol{\Psi}_{\text{o}}\} & \text{Re}\{\boldsymbol{\Psi}_{\text{o}}\} \end{bmatrix} \qquad \in \mathbb{R}^{2n \times 2(n+\widetilde{M})} \tag{4.14}$$

$$\tilde{\boldsymbol{x}}_{\text{ML}} = \begin{bmatrix} \text{Re}\{\tilde{\boldsymbol{x}}\} \\ \text{Im}\{\tilde{\boldsymbol{x}}\} \end{bmatrix} \qquad \in \mathbb{R}^{2(n+\widetilde{M})} \tag{4.15}$$

$$\tag{4.16}$$

We also redefine the $|\cdot|^{\circ 2}_{\text{ML}}$ operator as:

$$\left|\cdot\right|^{\circ 2}_{\text{ML}} : \mathbb{R}^{2n} \to \mathbb{R}^{n} \tag{4.17}$$

$$\left| \begin{bmatrix} x_1 \\ \vdots \\ x_{2n} \end{bmatrix} \right|^{\circ 2}_{\text{ML}} = \begin{bmatrix} x_1^2 + x_{1+n}^2 \\ \vdots \\ x_n^2 + x_{2n}^2 \end{bmatrix} \tag{4.18}$$

In this way, the system model is completely reparametrized into an analogous and completely real-valued problem:

$$\boldsymbol{y}_{\text{e}} = |\boldsymbol{\Psi}_{\text{e,ML}} \tilde{\boldsymbol{x}}_{\text{ML}}|^{\circ 2}_{\text{ML}} + \boldsymbol{n}_{\text{e}} \qquad \in \mathbb{R}^{n} \tag{4.19}$$

$$\boldsymbol{y}_{\text{o}} = |\boldsymbol{\Psi}_{\text{o,ML}} \tilde{\boldsymbol{x}}_{\text{ML}}|^{\circ 2}_{\text{ML}} + \boldsymbol{n}_{\text{o}} \qquad \in \mathbb{R}^{n} \tag{4.20}$$

4.3 MagPhase-DetNet architecture

Now we are going to construct the architecture of the decoder based on the machine Learning solution presented in [12], hence, from now on, all the matrices and the $|\cdot|^{\circ 2}$ operator are to be understood as the reparametrized version of the problem, that means as if they have the subscript "ML" even if they do not.

The detection problem, according to the maximum likelihood criterion, is given by:

$$\hat{\tilde{\boldsymbol{x}}}' = \arg \min_{\tilde{\boldsymbol{x}}' \in \mathbb{K}^{2n}} \left\| \boldsymbol{y} - \left| \boldsymbol{\Psi} \tilde{\boldsymbol{x}}' \right|^{\circ 2} \right\|^2 \tag{4.21}$$

which, using the separation of channels, is equivalent to:

$$\hat{\tilde{\boldsymbol{x}}} = \arg \min_{\tilde{\boldsymbol{x}} \in \mathbb{K}^{n}} \left\{ \left\| \boldsymbol{y}_{\text{e}} - |\boldsymbol{\Psi}_{\text{e}} \tilde{\boldsymbol{x}}|^{\circ 2} \right\|^2 + \left\| \boldsymbol{y}_{\text{o}} - |\boldsymbol{\Psi}_{\text{o}} \tilde{\boldsymbol{x}}|^{\circ 2} \right\|^2 \right\} \tag{4.22}$$

Given this objective function, in [12], it is recommended to use the gradient of the expression above in the architecture, so each layer of the DetNet should mimic one projected gradient descent step, that is:

$$\tilde{\boldsymbol{x}}_{k+1} = \Pi \left(\tilde{\boldsymbol{x}}_k + \delta_k \nabla_{\tilde{\boldsymbol{x}}} \boldsymbol{f}(\tilde{\boldsymbol{x}}) \big|_{\tilde{\boldsymbol{x}} = \tilde{\boldsymbol{x}}_k} \right)$$

$$\text{whith} \quad \boldsymbol{f}(\tilde{\boldsymbol{x}}) = \left\| \boldsymbol{y}_{\text{e}} - |\boldsymbol{\Psi}_{\text{e}} \tilde{\boldsymbol{x}}|^{\circ 2} \right\|^2 + \left\| \boldsymbol{y}_{\text{o}} - |\boldsymbol{\Psi}_{\text{o}} \tilde{\boldsymbol{x}}|^{\circ 2} \right\|^2$$

where $\Pi(\cdot)$ is a nonlinear function that forces the gradient descent to be a possible solution, which means $\hat{\boldsymbol{x}}_{k+1} \in \mathbb{K}^n$.

However, we tried this approach with several small variations in the loss function and the projection function, and we got no good results; this shows that the approach is not good, so we had to find a better one.

We noticed that for the DD system, it is straightforward to detect the magnitude of the symbols (that is what a normal IM-DD system does), but the phase detection is the big problem. Also along all the studied papers is present the idea that one sample carries the information about the magnitude and the other carries, somehow, the information about the phase. Even in [6], the magnitude and phase detection are treated almost as separate tasks.

With this in mind, we decided to separate the two tasks a little, so we propose the architecture shown in figure 4.1. The idea is to use one DetNet-based block on each layer to improve the magnitude estimate (without changing the phase), followed by a DetNet-based block to improve the phase estimate (without changing the magnitude) and concatenate many layers to get the final architecture.

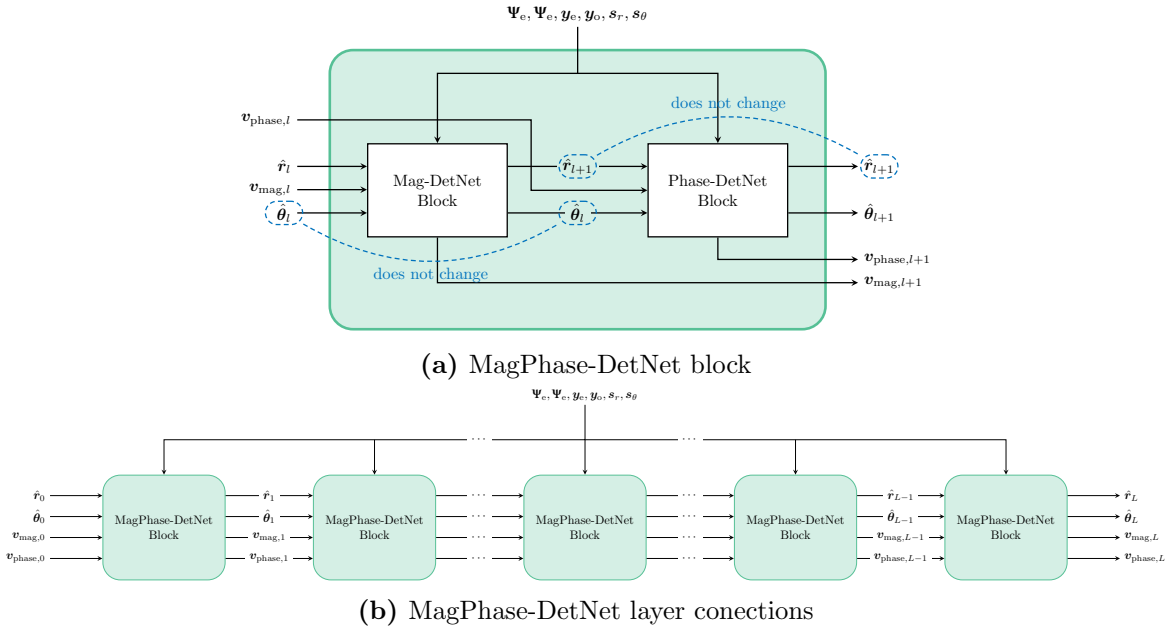

(a) MagPhase-DetNet block

(b) MagPhase-DetNet layer conections

Figure 4.1: MagPhase-DetNet architecture.

4.3.1 Magnitude phase reparametrization

Before defining the architecture in detail, we have to do a small reparametrization of $\boldsymbol{x}$ from cartesian to polar form as follows:

$$\tilde{\boldsymbol{x}} = \begin{bmatrix} \boldsymbol{r} \\ \boldsymbol{r} \end{bmatrix} \odot \begin{bmatrix} \cos(\boldsymbol{\theta}) \\ \sin(\boldsymbol{\theta}) \end{bmatrix} \tag{4.23}$$

with $\boldsymbol{r}, \boldsymbol{\theta} \in \mathbb{R}^{n+\widetilde{M}}$ contains the magnitude and phase of each symbol, the cosine and sine are applied element-wise, and the $\odot$ operator is the elementwise multiplication.

If we define $\boldsymbol{R}(\boldsymbol{r}) = \begin{bmatrix}\boldsymbol{r} & \boldsymbol{r}\end{bmatrix}^T$ and $\boldsymbol{w}(\boldsymbol{\theta}) = \begin{bmatrix}\cos(\boldsymbol{\theta}) & \sin(\boldsymbol{\theta})\end{bmatrix}^T$, the element-wise product is equivalent to the next two matrix-vector multiplications:

$$\tilde{X} = \boldsymbol{R}(\boldsymbol{r}) \odot \boldsymbol{w}(\boldsymbol{\theta}) = \operatorname{diag}\big(\boldsymbol{R}(\boldsymbol{r})\big) \cdot \boldsymbol{w}(\boldsymbol{\theta}) = \operatorname{diag}\big(\boldsymbol{w}(\boldsymbol{\theta})\big) \cdot \boldsymbol{R}(\boldsymbol{r}) \tag{4.24}$$

which are useful to calculate the gradients.

4.3.2 Magnitude DetNet block

For the magnitude block, each block should perform a gradient descent step with respect to the magnitude of the symbols, and assuming the phases constant, the first step to define the block structure is to calculate the following gradient:

$$\nabla_{\boldsymbol{r}} \left\| \boldsymbol{y}_{\mathrm{e}} - |\boldsymbol{\Psi}_{\mathrm{e}}\tilde{\boldsymbol{x}}|^{\circ 2} \right\|^2 + \left\| \boldsymbol{y}_{\mathrm{o}} - |\boldsymbol{\Psi}_{\mathrm{o}}\tilde{\boldsymbol{x}}|^{\circ 2} \right\|^2 \tag{4.25}$$

$$= \nabla_{\boldsymbol{r}} \left\| \boldsymbol{y}_{\mathrm{e}} - \left|\boldsymbol{\Psi}_{\mathrm{e}} \cdot \operatorname{diag}\big(\boldsymbol{w}(\boldsymbol{\theta})\big) \cdot \boldsymbol{R}(\boldsymbol{r})\right|^{\circ 2} \right\|^2 + \left\| \boldsymbol{y}_{\mathrm{o}} - \left|\boldsymbol{\Psi}_{\mathrm{o}} \cdot \operatorname{diag}\big(\boldsymbol{w}(\boldsymbol{\theta})\big) \cdot \boldsymbol{R}(\boldsymbol{r})\right|^{\circ 2} \right\|^2 \tag{4.26}$$

which we will name $\mathrm{grad}_{\mathrm{mag}}$, and after some calculations we get:

$$\mathrm{grad}_{\mathrm{mag}} = \boldsymbol{A}_{\mathrm{e}} \cdot \left(2\boldsymbol{y}_{\mathrm{e}} - 2\,|\boldsymbol{\Psi}_{\mathrm{e}}\tilde{\boldsymbol{x}}|^{\circ 2}\right) + \boldsymbol{A}_{\mathrm{o}} \cdot \left(2\boldsymbol{y}_{\mathrm{o}} - 2\,|\boldsymbol{\Psi}_{\mathrm{o}}\tilde{\boldsymbol{x}}|^{\circ 2}\right) \tag{4.27}$$

where

$$\boldsymbol{A}_{\mathrm{e},l} = \begin{bmatrix}\operatorname{diag}\big(\cos(\boldsymbol{\theta})\big) & \operatorname{diag}\big(\sin(\boldsymbol{\theta})\big)\end{bmatrix} \cdot \boldsymbol{\Psi}_{\mathrm{e}}^T \cdot \begin{bmatrix} \operatorname{diag}\left(\left[2\boldsymbol{\Psi}_{\mathrm{e}}\tilde{\boldsymbol{x}}_l\right]_0^n\right) \\ \operatorname{diag}\left(\left[2\boldsymbol{\Psi}_{\mathrm{e}}\tilde{\boldsymbol{x}}_l\right]_n^{2n}\right) \end{bmatrix} \tag{4.28}$$

$$\boldsymbol{A}_{\mathrm{o},l} = \begin{bmatrix}\operatorname{diag}\big(\cos(\boldsymbol{\theta})\big) & \operatorname{diag}\big(\sin(\boldsymbol{\theta})\big)\end{bmatrix} \cdot \boldsymbol{\Psi}_{\mathrm{o}}^T \cdot \begin{bmatrix} \operatorname{diag}\left(\left[2\boldsymbol{\Psi}_{\mathrm{o}}\tilde{\boldsymbol{x}}_l\right]_0^n\right) \\ \operatorname{diag}\left(\left[2\boldsymbol{\Psi}_{\mathrm{e}}\tilde{\boldsymbol{x}}_l\right]_n^{2n}\right) \end{bmatrix} \tag{4.29}$$

where $[\cdot]_a^b$ denotes the the elements from position a to b (not included) of a vector, and the l subindex denotes the l-th layer of the network.

Now, following the procedure from [12], we give the architecture of the magnitude network, where each layer is given by:

$$\boldsymbol{r}_{l-1} = \begin{bmatrix} \boldsymbol{s}_r \\ \hat{\boldsymbol{r}}_{l-1} \end{bmatrix} \tag{4.30}$$

$$\boldsymbol{\theta}_{l-1} = \begin{bmatrix} \boldsymbol{s}_\theta \\ \hat{\boldsymbol{\theta}}_{l-1} \end{bmatrix} \tag{4.31}$$

$$\tilde{\boldsymbol{x}}_{l-1} = \boldsymbol{R}(\boldsymbol{r}_{l-1}) \odot \boldsymbol{w}(\boldsymbol{\theta}_{l-1}) \tag{4.32}$$

$$\begin{aligned} \boldsymbol{q}_l = \boldsymbol{r}_{l-1} - \delta_{1l}\boldsymbol{A}_{\mathrm{e},l-1}\boldsymbol{y}_\mathrm{e} + \delta_{2l}\boldsymbol{A}_{\mathrm{e},l-1}|\boldsymbol{\Psi}_\mathrm{e}\tilde{\boldsymbol{x}}_{l-1}|^{\circ 2} - \\ \delta_{3l}\boldsymbol{A}_{\mathrm{o},l-1}\boldsymbol{y}_\mathrm{o} + \delta_{4l}\boldsymbol{A}_{\mathrm{o},l-1}|\boldsymbol{\Psi}_\mathrm{o}\tilde{\boldsymbol{x}}_{l-1}|^{\circ 2} \end{aligned} \tag{4.33}$$

$$\boldsymbol{z}_l = \rho\left(\boldsymbol{W}_{1l}\begin{bmatrix} \boldsymbol{q}_l \\ \boldsymbol{v}_{l-1} \end{bmatrix} + \boldsymbol{b}_{1l}\right) \tag{4.34}$$

$$\boldsymbol{r}_{\mathrm{oh},l} = \boldsymbol{r}_{\mathrm{oh},l-1} + \boldsymbol{W}_{2l}\boldsymbol{z}_l + \boldsymbol{b}_{2l} \tag{4.35}$$

$$\hat{\boldsymbol{r}}_l = \left[\boldsymbol{f}_\mathrm{oh}(\boldsymbol{r}_{\mathrm{oh},l})\right]_{\widetilde{M}}^{\mathrm{end}} \tag{4.36}$$

$$\boldsymbol{v}_{\mathrm{mag},l} = \boldsymbol{v}_{\mathrm{mag},l-1} + \boldsymbol{W}_{3l}\boldsymbol{z}_l + \boldsymbol{b}_{3l} \tag{4.37}$$

$$\hat{\boldsymbol{r}}_0 = \boldsymbol{0} \tag{4.38}$$

$$\boldsymbol{v}_{\mathrm{mag},0} = \boldsymbol{0} \tag{4.39}$$

$$\tag{4.40}$$

where $\rho(\cdot)$ is the ReLu activation function, $\boldsymbol{W}$ a matrix and $\boldsymbol{b}$ a vector that together apply a linear transformation, the function $\boldsymbol{f}_\mathrm{oh}(\cdot)$ is as defined in [12] and $[\boldsymbol{c}]_m^{\mathrm{end}}$ denotes the elements of $\boldsymbol{c}$ from m to the last.

The trainable parameters of the model are:

$$\boldsymbol{\Theta}_\mathrm{mag} = \left\{\boldsymbol{W}_{1l}, \boldsymbol{b}_{1l}, \boldsymbol{W}_{2l}, \boldsymbol{b}_{2l}, \boldsymbol{W}_{3l}, \boldsymbol{b}_{3l}, \delta_{1l}, \delta_{2l}, \delta_{3l}, \delta_{4l}\right\}_{l=1}^{L} \tag{4.41}$$

where L is the number of layers, and the loss function used for training is:

$$\mathrm{loss}(\boldsymbol{r}, \hat{\boldsymbol{r}}(\boldsymbol{\Psi}_\mathrm{e}, \boldsymbol{\Psi}_\mathrm{e}, \boldsymbol{y}_\mathrm{e}, \boldsymbol{y}_\mathrm{o}, \boldsymbol{s}_r, \boldsymbol{s}_\theta; \boldsymbol{\Theta}_\mathrm{mag})) = \sum_{l=1}^{L} \log(l)\|\boldsymbol{r} - \hat{\boldsymbol{r}}_l\|^2 \tag{4.42}$$

4.3.3 Phase DetNet block

For the phase block, each block should perform a gradient descent step with respect to the phase of the symbols, so we follow the same procedure as for the magnitude block and calculate the following gradient:

$$\nabla_{\boldsymbol{\theta}} \left\| \boldsymbol{y}_\mathrm{e} - |\boldsymbol{\Psi}_\mathrm{e}\tilde{\boldsymbol{x}}|^{\circ 2} \right\|^2 + \left\| \boldsymbol{y}_\mathrm{o} - |\boldsymbol{\Psi}_\mathrm{o}\tilde{\boldsymbol{x}}|^{\circ 2} \right\|^2 \tag{4.43}$$

$$= \nabla_{\boldsymbol{\theta}} \left\| \boldsymbol{y}_\mathrm{e} - \left|\boldsymbol{\Psi}_\mathrm{e} \cdot \mathrm{diag}\big(\boldsymbol{R}(\boldsymbol{r})\big) \cdot \boldsymbol{w}(\boldsymbol{\theta})\right|^{\circ 2} \right\|^2 + \left\| \boldsymbol{y}_\mathrm{o} - \left|\boldsymbol{\Psi}_\mathrm{o} \cdot \mathrm{diag}\big(\boldsymbol{R}(\boldsymbol{r})\big) \cdot \boldsymbol{w}(\boldsymbol{\theta})\right|^{\circ 2} \right\|^2 \tag{4.44}$$

which we will name $\mathrm{grad}_\mathrm{phase}$, and after some calculations we get:

$$\mathrm{grad}_\mathrm{phase} = \boldsymbol{A}_\mathrm{e} \cdot \left(2\boldsymbol{y}_\mathrm{e} - 2\left|\boldsymbol{\Psi}_\mathrm{e}\tilde{\boldsymbol{x}}\right|^{\circ 2}\right) + \boldsymbol{A}_\mathrm{o} \cdot \left(2\boldsymbol{y}_\mathrm{o} - 2\left|\boldsymbol{\Psi}_\mathrm{o}\tilde{\boldsymbol{x}}\right|^{\circ 2}\right) \tag{4.45}$$

where

$$\boldsymbol{A}_{\mathrm{e},l} = \begin{bmatrix} -\mathrm{diag}\left(\left[\tilde{\boldsymbol{x}}_l\right]_n^{2n}\right) & \mathrm{diag}\left(\left[\tilde{\boldsymbol{x}}_l\right]_0^{n}\right) \end{bmatrix} \cdot \boldsymbol{\Psi}_{\mathrm{e}}^T \cdot \begin{bmatrix} \mathrm{diag}\left(\left[2\boldsymbol{\Psi}_{\mathrm{e}}\tilde{\boldsymbol{x}}_l\right]_0^{n}\right) \\ \mathrm{diag}\left(\left[2\boldsymbol{\Psi}_{\mathrm{e}}\tilde{\boldsymbol{x}}_l\right]_n^{2n}\right) \end{bmatrix} \tag{4.46}$$

$$\boldsymbol{A}_{\mathrm{e},l} = \begin{bmatrix} -\mathrm{diag}\left(\left[\tilde{\boldsymbol{x}}_l\right]_n^{2n}\right) & \mathrm{diag}\left(\left[\tilde{\boldsymbol{x}}_l\right]_0^{n}\right) \end{bmatrix} \cdot \boldsymbol{\Psi}_{\mathrm{e}}^T \cdot \begin{bmatrix} \mathrm{diag}\left(\left[2\boldsymbol{\Psi}_{\mathrm{e}}\tilde{\boldsymbol{x}}_l\right]_0^{n}\right) \\ \mathrm{diag}\left(\left[2\boldsymbol{\Psi}_{\mathrm{e}}\tilde{\boldsymbol{x}}_l\right]_n^{2n}\right) \end{bmatrix} \tag{4.47}$$

where $[\cdot]_a^b$ denotes the the elements from position a to b (not included) of a vector.

Now, following the procedure from [12], we give the architecture of the phase network, where each layer is given by:

$$\boldsymbol{r}_{l-1} = \begin{bmatrix} \boldsymbol{s}_r \\ \hat{\boldsymbol{r}}_{l-1} \end{bmatrix} \tag{4.48}$$

$$\boldsymbol{\theta}_{l-1} = \begin{bmatrix} \boldsymbol{s}_\theta \\ \hat{\boldsymbol{\theta}}_{l-1} \end{bmatrix} \tag{4.49}$$

$$\tilde{\boldsymbol{x}}_{l-1} = \boldsymbol{R}(\boldsymbol{r}_{l-1}) \odot \boldsymbol{w}(\boldsymbol{\theta}_{l-1}) \tag{4.50}$$

$$\begin{aligned} \boldsymbol{q}_l = \boldsymbol{\theta}_{l-1} - \delta_{1l}\boldsymbol{A}_{\mathrm{e},l-1}\boldsymbol{y}_{\mathrm{e}} + \delta_{2l}\boldsymbol{A}_{\mathrm{e},l-1}|\boldsymbol{\Psi}_{\mathrm{e}}\tilde{\boldsymbol{x}}_{l-1}|^{\circ 2} - \\ \delta_{3l}\boldsymbol{A}_{\mathrm{o},l-1}\boldsymbol{y}_{\mathrm{o}} + \delta_{4l}\boldsymbol{A}_{\mathrm{o},l-1}|\boldsymbol{\Psi}_{\mathrm{o}}\tilde{\boldsymbol{x}}_{l-1}|^{\circ 2} \end{aligned} \tag{4.51}$$

$$\boldsymbol{z}_l = \rho\left(\boldsymbol{W}_{1l}\begin{bmatrix} \boldsymbol{q}_l \\ \boldsymbol{v}_{l-1} \end{bmatrix} + \boldsymbol{b}_{1l}\right) \tag{4.52}$$

$$\boldsymbol{\theta}_{\mathrm{oh},l} = \boldsymbol{\theta}_{\mathrm{oh},l-1} + \boldsymbol{W}_{2l}\boldsymbol{z}_l + \boldsymbol{b}_{2l} \tag{4.53}$$

$$\hat{\boldsymbol{\theta}}_l = \left[\boldsymbol{f}_{\mathrm{oh}}(\boldsymbol{\theta}_{\mathrm{oh},l})\right]_{\widetilde{M}}^{\mathrm{end}} \tag{4.54}$$

$$\boldsymbol{v}_{\mathrm{phase},l} = \boldsymbol{v}_{\mathrm{phase},l-1} + \boldsymbol{W}_{3l}\boldsymbol{z}_l + \boldsymbol{b}_{3l} \tag{4.55}$$

$$\hat{\boldsymbol{\theta}}_0 = \boldsymbol{0} \tag{4.56}$$

$$\boldsymbol{v}_{\mathrm{phase},0} = \boldsymbol{0} \tag{4.57}$$

$$\tag{4.58}$$

where $\rho(\cdot)$ is the ReLu activation function, $\boldsymbol{W}$ a matrix and $\boldsymbol{b}$ a vector that together applies a linear transformation, and the function $\boldsymbol{f}_{\mathrm{oh}}(\cdot)$ is as defined in [12].

The trainable parameters of the model are:

$$\boldsymbol{\Theta}_{\mathrm{phase}} = \left\{\boldsymbol{W}_{1l}, \boldsymbol{b}_{1l}, \boldsymbol{W}_{2l}, \boldsymbol{b}_{2l}, \boldsymbol{W}_{3l}, \boldsymbol{b}_{3l}, \delta_{1l}, \delta_{2l}, \delta_{3l}, \delta_{4l}\right\}_{l=1}^{L} \tag{4.59}$$

where L is the number of layers, and the loss function used for training is:

$$\mathrm{loss}(\boldsymbol{\theta}, \hat{\boldsymbol{\theta}}(\boldsymbol{\Psi}_{\mathrm{e}}, \boldsymbol{\Psi}_{\mathrm{e}}, \boldsymbol{y}_{\mathrm{e}}, \boldsymbol{y}_{\mathrm{o}}, \boldsymbol{s}_r, \boldsymbol{s}_\theta; \boldsymbol{\Theta}_{\mathrm{phase}})) = \sum_{l=1}^{L} \log(l)\|\boldsymbol{\theta} - g_{\text{diff deco}}(\hat{\boldsymbol{\theta}}_l)\|^2 \tag{4.60}$$

where $g_{\text{diff deco}}(\cdot)$ is a function that implements the differential decoding and depends on the constellation used.

4.4 Numerical simulation

To implement the proposed architecture, we used the Pytorch framework, the code can be found in the GitHub repository Direct_Detection_with_Phase_Recovery. For training as well as evaluating the network we use the simulation parameters shown in table 3.1, the constellation used is DD-SQAM, and we focused on the case when the auxiliary channel and real channel are equal, i.e. $\widetilde{N} = \widetilde{M}$, in particular for $\widetilde{M} = 1, 3, 5$. Finally, we considered the SNR range from 0 dB to 20 dB, and for each SNR and $\widetilde{M}$ a different model is trained.

4.4.1 Training process

4.4.1.1 Hyper parameters

For the architecture, we used the following lengths of the vectors and number of layers:

$$\text{len}(\tilde{\boldsymbol{x}}) = 2\widetilde{M} + 1 \tag{4.61}$$

$$\text{len}(\boldsymbol{v}) = 2 \cdot (2\widetilde{M} + 1) \tag{4.62}$$

$$\text{len}(\boldsymbol{z}) = 4 \cdot (2\widetilde{M} + 1) \tag{4.63}$$

$$L = \max(3 \cdot (2\widetilde{M} + 1), 30) \tag{4.64}$$

where len$(\cdot)$ denotes the length of the vector and max() returns the biggest element of the argument.

4.4.1.2 Training set

The training set consists of the output of the system after simulating the transmission of $2\widetilde{M} + 1$ random symbols, where the first $\widetilde{M}$ represents the state of the channel, and the last $\widetilde{M} + 1$ symbols are transmitted symbols. As a result, the network should be trained for all possible states and transmitted symbols.

For the training we use a variable batch size that takes the following values in order $[100, 400, 1000, 2000, 5000, 10000]$ and performs 300 learning processes for each batch size.

4.4.2 Evaluation process

4.4.2.1 Simple evaluation

For the evaluation process, we perform two evaluations. The first one is an evaluation equal to training, which means using many small transmissions of $2\widetilde{M} + 1$ symbols, where the first $\widetilde{M}$ symbols represent the state of the channel and are passed to the MagPhase-DetNet as an input (that means assuming perfect channel state knowledge). We evaluate only the SER of the next symbol as shown in figure 4.2. We do this because we noticed that the reliability of the detection decreases for the last symbols.

After doing this and plotting the results, we get the graph of figure 4.3, which shows the performance, in terms of SER, of the models trained for each channel memory and SNR. The graph is to be interpreted as the best performance that the architecture can achieve when trained for a specific SNR.

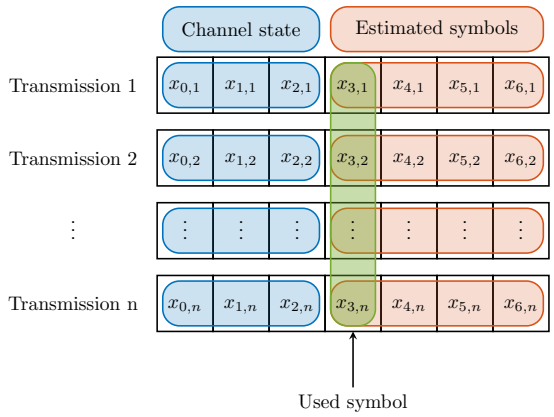

Figure 4.2: Evaluation method used for the simple evaluation of the MagPhase-DetNet. Example for $\widetilde{M} = 3$.

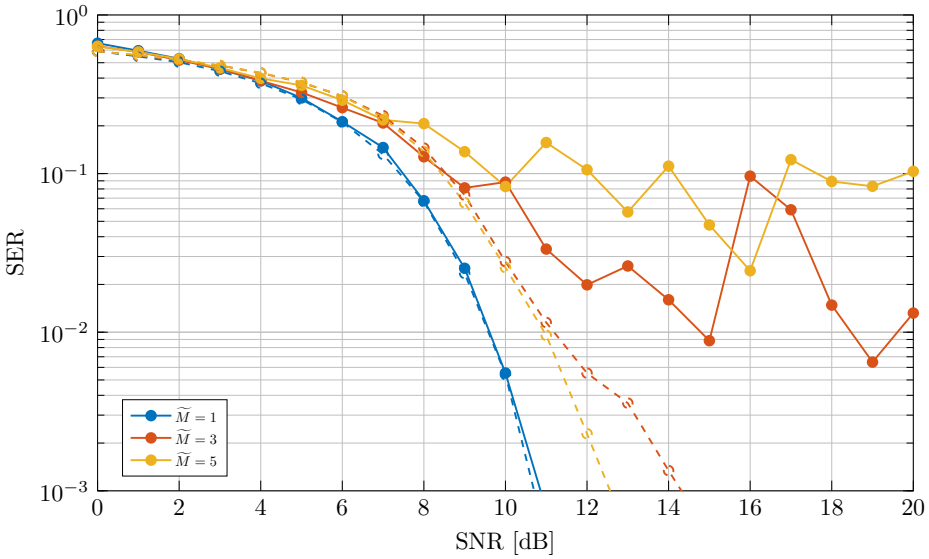

Figure 4.3: Simple evaluation of the MagPhase-DetNet trained for different SNR and channel memory. The dotted lines are the reference optimal performance.

Analyzing the results, it is easy to notice that for the $\widetilde{M} = 1$ case, the performance of the MagPhase-DetNet is almost optimal. In contrast, for $\widetilde{M} = 3$ and 5, the performance is near to the optimal only for slow SNR; at bigger SNR, the architecture tends to have an error floor. Also, it is important to note that the graph is not smooth, this could happen because the training process was insufficient.

4.4.2.2 Sequential evaluation

The next test tries to implement the network as it would be implemented in a practical application, where one does not have access to different transmission segments with perfect channel knowledge but only to a long string of samples. That is why we use the network as shown in figure 4.4, we start with an initial channel knowledge and use the network to

decode the next symbol. Then, we use the decoded symbol to determine the new state of the channel and, with it, decode the next symbol. The process continues until the end of the transmission.

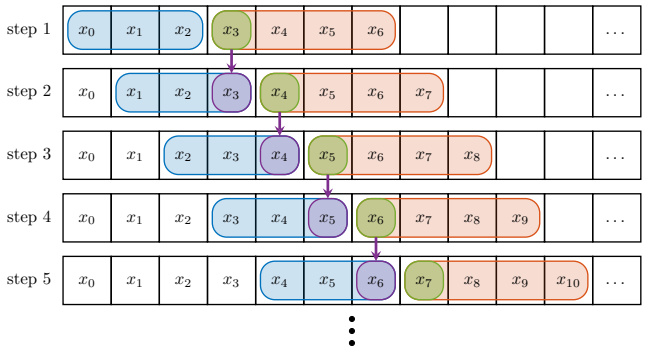

Figure 4.4: Evaluation method used for the sequential evaluation of the MagPhase-DetNet. Example for $\widetilde{M} = 3$.

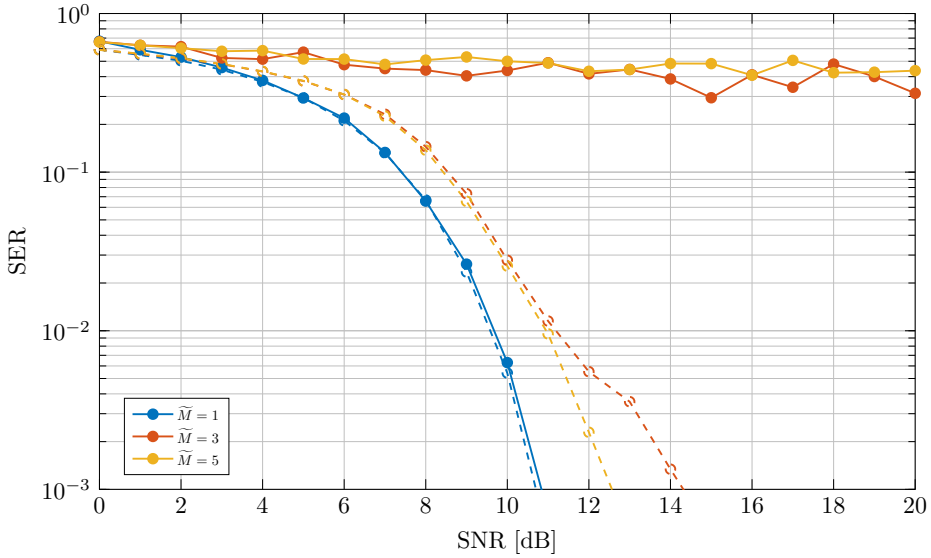

Figure 4.5: Sequential evaluation of the MagPhase-DetNet trained for different SNR and channel memory. The dotted lines are the reference optimal performance.

The performance for the $\widetilde{M} = 1$ case is again almost optimal. However, the other two cases are bad because they show a big error floor. Nevertheless, the error floor is below 3/4, meaning the decoding system is better than randomly guessing the symbols. This suggests that the system tries to work, but severe error propagation may degrade the performance. This shows that the proposed architecture depends on the quality of the channel state knowledge, and a small error can propagate a lot.

4.5 Conclusions

After watching the trained MagPhase-DetNet network's performance, it is evident that the performance is not as good as needed because the trained models (except for the trivial case

$\widetilde{M}$) present a high error floor at high SER, which means that the architecture proposed in this chapter is not the most appropriate.

However, the simple evaluation in figure 4.3 has a decent performance, which shows that a machine learning-based system may solve the problem but at the expense of needing a big training phase. Also, looking at the sequential evaluation in figure 4.5, one can notice that the decent performance of the first case is completely lost. This shows that the network fails when it tries to generalize to the sequential case, so to improve the model, one should modify the architecture to make it compatible with the sequential nature of the transmission.

For example, a possible solution to improve the architecture in the sequential case is to use a convolutional neural network; because the underlying nature of the system is a convolution, it is reasonable to think that a convolutional network may have some advantages. This is an exciting topic for future work: exploring new architecture better suited for the problem.

Also, we see that the training cost of these machine learning-based decoders grows rapidly with an increasing channel memory, which is why the graphs in figure 4.3 are not smooth. With this in mind, another exciting field of work is to design a new pulse waveform that compromises the bandwidth and the channel memory.

This page intentionally left blank.

Bibliography

[1] A. Tasbihi and F. R. Kschischang, "Direct detection under tukey signalling," *Journal of Lightwave Technology*, vol. 39, no. 21, pp. 6845–6857, 2021. DOI: 10.1109/JLT.2021.3109852.

[2] G. P. Agrawal, "Introduction," in *Fiber-Optic Communication Systems*. John Wiley & Sons, Ltd, 2010, ch. 1, pp. 1–23, ISBN: 9780470918524. DOI: https://doi.org/10.1002/9780470918524.ch1. eprint: https://onlinelibrary.wiley.com/doi/pdf/10.1002/9780470918524.ch1. [Online]. Available: https://onlinelibrary.wiley.com/doi/abs/10.1002/9780470918524.ch1.

[3] A. Mecozzi and M. Shtaif, "Information capacity of direct detection optical transmission systems," *Journal of Lightwave Technology*, vol. 36, no. 3, pp. 689–694, 2018. DOI: 10.1109/JLT.2017.2777188.

[4] G. P. Agrawal, "Optical receivers," in *Fiber-Optic Communication Systems*. John Wiley & Sons, Ltd, 2010, ch. 4, pp. 128–181, ISBN: 9780470918524. DOI: https://doi.org/10.1002/9780470918524.ch4. eprint: https://onlinelibrary.wiley.com/doi/pdf/10.1002/9780470918524.ch4. [Online]. Available: https://onlinelibrary.wiley.com/doi/abs/10.1002/9780470918524.ch4.

[5] A. Tasbihi and F. R. Kschischang, "On the capacity of waveform channels under square-law detection of time-limited signals," *IEEE Transactions on Information Theory*, vol. 66, no. 11, pp. 6682–6687, 2020. DOI: 10.1109/TIT.2020.2999889.

[6] M. Secondini and E. Forestieri, "Direct detection of bipolar pulse amplitude modulation," *Journal of Lightwave Technology*, vol. 38, no. 21, pp. 5981–5990, 2020. DOI: 10.1109/JLT.2020.3007584.

[7] D. Plabst, T. Prinz, T. Wiegart, *et al.*, "Achievable rates for short-reach fiber-optic channels with direct detection," *Journal of Lightwave Technology*, vol. 40, no. 12, pp. 3602–3613, 2022. DOI: 10.1109/JLT.2022.3149574.

[8] D. J. C. MacKay, *Information theory, inference, and learning algorithms*, 15th print. Cambridge [u.a.]: Cambridge University Press, 2015, ISBN: 9780521642989. [Online]. Available: http://bvbr.bib-bvb.de:8991/F?func=service&doc_library=BVB01&doc_number=020774035&line_number=0001&func_code=DB_RECORDS&service_type=MEDIA.

[9] T. Prinz, D. Plabst, T. Wiegart, S. Calabrò, N. Hanik, and G. Kramer, *Successive interference cancellation for bandlimited channels with direct detection*, 2023. arXiv: 2212.07761 [cs.IT].

[10] T. Wang, T. Lv, H. Gao, and S. Zhang, "Joint multiple symbol differential detection and channel decoding for noncoherent uwb impulse radio by belief propagation," *IEEE Transactions on Wireless Communications*, vol. 16, no. 1, pp. 293–306, 2017. DOI: 10.1109/TWC.2016.2623301.

[11] N. Samuel, T. Diskin, and A. Wiesel, "Deep mimo detection," in *2017 IEEE 18th International Workshop on Signal Processing Advances in Wireless Communications (SPAWC)*, 2017, pp. 1–5. DOI: 10.1109/SPAWC.2017.8227772.

[12] N. Samuel, T. Diskin, and A. Wiesel, "Learning to detect," *IEEE Transactions on Signal Processing*, vol. 67, no. 10, pp. 2554–2564, 2019. DOI: 10.1109/TSP.2019.2899805.